Structure-Function Relationships in Polymeric Multilayer Capsules Designed for Cancer Drug Delivery

Galina Nifontova, Tatiana Tsoi, Alexander Karaulov, Igor Nabiev, Alyona Sukhanova

ARTICLE

Structure–Function Relationships in Polymeric Multilayer Capsules Designed for Cancer Drug Delivery

Received 00th January 20xx,
Accepted 00th January 20xx

DOI: 10.1039/x0xx00000x

Galina Nifontova[†a], Tatiana Tsoi[†b], Alexander Karaulov[c], Igor Nabiev*[a,b,c], and Alyona Sukhanova*[a]

Targeted delivery of cancer drugs to tumor-specific molecular targets represents a major challenge in modern personalized cancer medicine. Engineering of micron and submicron polymeric multilayer capsules allows obtaining multifunctional theranostic systems serving as controllable stimulus-responsive tools with a high clinical potential to be used in cancer therapy and detection. The functionalities of such theranostic systems are determined by the design and structural properties of the capsules. This review (1) describes the current issues in designing cancer cell–targeting polymeric multilayer capsules, (2) analyzes the effects of the interactions of the capsules with the cellular and molecular constituents of biological fluids, and (3) presents the key structural parameters determining the effectiveness of capsules targeting. The influence of the morphological and physicochemical parameters and the origin of structural components and surface ligands on the functional activity of polymeric multilayer capsules at the molecular, cellular, and whole-body levels are summarized. The basic structural and functional principles determining the future trends of theranostic capsule development are established and discussed.

1. Introduction

Novel approaches to safer and more controllable anticancer therapy are aimed at enhancing the therapeutic potential of anticancer agents and reducing their toxicity. Current research and developments are focused on designing novel cancer cell–targeted delivery platforms, including nano- and microparticles, implants, scaffolds, biomaterials, and cell-based platforms.

Multilayer capsules represent multi-purpose containers that can be used in biomedical applications, including controlled targeted delivery [1–3], theranostics [4], sensing [5–8], microreactors [9], nanophotonics, and imaging [10,11].

The approaches to the preparation of multilayer structures include traditional techniques, such as layer-by-layer assembly [12], as well as the novel and more technologically advanced fluidic approach [13,14], emulsion [15], fluidized-bed coating [16–18], ultrasonic atomization [19], and electro-spraying [20]. The assembly of the multilayer capsules is based on coating various templates with polymers. Rigid templates, such as crystals (e.g., calcium carbonate [12,13,21–26] and manganese carbonate [27]), zeolitic imidazolate frameworks [28], and silica spheres [13,16,29–31] of various sizes, shapes, and structures, are classical templates for depositing polymer multilayers. However, soft templates, e.g., hydrogels [32], micelles [33], organosolv nanoparticles [27], and stabilized emulsions [34–36], have been shown to be effective alternatives to solid templates, providing the opportunity for microfluidic approaches to be extensively used for polymer layering. Linear [21,28,32,37,38], branched [33], and/or grafted [36] polyelectrolyte polymers or polymer mixtures [39,40] are extensively used in capsule shell formation. Attachment of various functional groups to these polymers makes it possible to modify both the inner structure and the surface of the capsule membrane. Versatility of the materials used in assembling the multilayer capsules ensures their biocompatibility defined as a low cytotoxicity, sufficient structural integrity, and biodegradability [21,41,42].

The multilayer structures can be adapted for specific applications by tuning the particle size, shape [32], design (the number of layers, shell or core/shell structure, embedment of other functional elements, etc.) [30,43,44], rigidity, and surface properties [45]. Engineering of the multilayer capsules allows obtaining multi-purpose systems serving as stimulus-responsive and controllable tools with a high biomedical potential to be used in clinic, in particular, for cancer therapy and diagnosis [11,45,46]. The existing approaches to multilayering and encapsulation enable effective entrapment of low-molecular-weight anticancer drugs (including doxorubicin [38,47,48], 5-fluorouracil [49], curcumin [42], thymoquinone [50], and

[a] Laboratoire de Recherche en Nanosciences, LRN-EA4682, Université de Reims Champagne-Ardenne, 51100 Reims, France.
[b] National Research Nuclear University MEPhI (Moscow Engineering Physics Institute), 115409 Moscow, Russia.
[c] Sechenov First Moscow State Medical University (Sechenov University), 119146 Moscow, Russia.
† Equal contribution.

Electronic Supplementary Information (ESI) available: [details of any supplementary information available should be included here]. See DOI: 10.1039/x0xx00000x

gemcitabine [46]), and high-molecular-weight compounds, such as enzymes [51], small interfering RNAs (siRNAs) [41,52], and antibodies [53], as well as nanoparticles representing drug–adjuvant complexes, e.g., doxorubicin–bovine serum albumin (BSA) conjugates [54], in multilayer containers.

Targeted delivery of the multilayer capsule–based systems to tumor molecular targets still represents a major challenge in modern personalized cancer medicine. The capsule surface charge and particle surface functionalization determine the possibility of their internalization by cancer cells. For cancer targeting, specific ligands characterized by affinity to tumor molecular targets are extensively used in the design of the particle surface to enable the particle accumulation and retention in the tumor growth area [55–57].

When capsule dispersions are administered intravascularly and the particles are migrating to their specific tumor molecular targets, the particles interact with components of blood, such as proteins, lipids, and cells [2,58,59]. As a result of the interaction of chemical groups on the surface of multilayer capsules and functional groups of proteins, protein clusters are formed on the surface of the particles. Classical plasma proteins, extracellular matrix proteins, proteins secreted into body fluids other than plasma, vesicular proteins, proteins of the outer cell surface, and various non-categorical proteins are the major compounds involved in the capsule opsonization [60–62]. However, in the case of the capsule surface opsonization, the effectiveness of the interaction of targeted capsules with cells may either decrease or increase [59]. Capsule opsonization directly affects the effectiveness of the delivery and interaction of targeted capsules with cells, which may result in a decrease or increase in the cancer cell targeting capacity of the multilayer capsules developed. Along with opsonization, the interaction of the capsules with immune system components, such as macrophages and T cells, as well as blood clotting factors and other components of biological fluids, should be considered in discussing the cancer cell targeting capacity, biodistribution, and tumor accumulation of these delivery vehicles [38,58,63]. The technologies of the synthesis of multilayer structures and methods of their encapsulation are rapidly improving and allow designing versatile stimulus-sensitive targeted systems serving as anticancer therapeutic tools. Recent reviews are mainly focused on the designing and functionalization of capsule-based delivery tools consisting of metal nanoparticles, drugs, and vector molecules [64–66]. However, the issues of capsule design, their targeted delivery to cancer cells, and their biointeractions are still rarely discussed [67]. Therefore, comprehensive systematic analysis of the influence of the multilayer capsule design on both opsonization of the capsules and their interaction with blood constituents and cancer cells is called for. The aim of this paper is to provide an overview of the state-of-the-art approaches to the functionalization of multilayer capsule–based delivery systems for cancer cell targeting and to analyze the effects of their interaction with cellular and molecular constituents of biological fluids, including opsonization, and the effectiveness of their targeted delivery to cancer cells. The key characteristics of capsule delivery systems that determine the effectiveness of their targeted delivery, including their functional components, size, shape, surface charge, and biofunctionalization with additional ligands or hydrophilic polymers, as well as the major factors of their uptake by cancer cells, are summarized.

2. Versatility of polymeric multilayer capsules as cancer cell–targeted delivery tools

2.1. Capsule structural components

One of the conditions for engineering an effective and safe drug delivery system based on multilayer capsules and targeted against cancer cells is the use of biocompatible and biodegradable materials and structural elements in their fabrication [42,68–70]. The use of nontoxic, biodegradable polymers and templates can improve the capsule design and enable controlled release of the encapsulated molecular cargos under the conditions specific for cancer cells and tumor growth area (pH, redox potential, etc.) or ensure the delivery to a specific cellular compartment, e.g., the cytoplasm or nucleus [42,46,47].

Considering the fluctuations of the pH values under normal blood conditions (7.4) and a slightly acidic pH of the tumor microenvironment (6.5–6.8) and intracellular medium (5.0–6.0), the pH-driven changes in capsule permeability for low- and high-molecular-weight compounds have been established [71]. The changes in capsule permeability regulated by pH are related to rearrangements in the polymer coating due to protonation/deprotonation of polymer chains that result in an increased porosity of the capsule shell [71–73]. The majority of the polyelectrolyte polymers extensively used in capsule assembling have pKa values that ensure permeability switching of the shell composed of them under certain physiological conditions [69,74,75]. For example, pH responsiveness of multilayer chitosan (CHI)/alginate (ALG) films has been observed as reversible multilayer restructuring in the pH range of 4.0–8.0, with a specific permeability pattern of the polyelectrolyte coating at pH 3.0–5.5 [76]. Multilayer capsules consisting of nondegradable polymers, including poly(sodium 4-styrenesulfonate) (PSS) and poly(allylamine hydrochloride) (PAH), and the degradable dextran sulfate sodium salt (DEXS) and poly-L-arginine hydrochloride (PARG) exhibited similar pH sensitivity behaviors in the pH range from 3.0 to 7.5, with a shift in the range between 4.5 and 6.0 [77]. The degradation kinetics of $(PARG/ALG)_2$/$(PARG/ALG)_2PARG$ capsules coated with the Eudragit L100 anionic copolymer of methacrylic acid and methyl methacrylate has been found to be pH-dependent and affected by enzymes, in particular, pronase. The capsules displayed no acute toxicity during 48 h at doses of 10–1000 capsules per cell [42]. Biodegradable multilayer PARG/DEXS capsules can be degraded by cells and eliminated from the body within 72 h. Their gradual degradation results in the formation of minute fragments of the capsule shell, which are observed in the intracellular space after the capsules have been internalized by cancer cells [25]. The polymers generally used as biocompatible and biodegradable capsule structural

components are listed in Fig. 1. Template particles used in the preparation of core/shell multilayer capsules should consist of environment-friendly materials; in the case of shell capsules, these templates should not require the use of highly toxic solvents for their removal. From this point of view, calcium carbonate templates represent an appropriate biomaterial, because their size, shape, crystal structure, and surface properties can be varied [78,79]. Calcium carbonate particles with spherical, elliptic, and toroid shapes do not exhibit any cytotoxicity even at a dose of 100 particles per cell [80]. Hollow soft capsules representing calcium carbonate particle replicas can be produced by dissolving the template core with ethylenediaminetetraacetic acid (EDTA) or hydrochloric acid, which is a green route for capsule engineering [25,81], whereas in the case of silica templates, which are also widely used in capsule manufacturing, the highly hazardous hydrofluoric acid serves as a solvent for core removal [82]. When the templates are polystyrene microparticles, organic solvents, such as tetrahydrofuran, have to be used to decompose the capsule core [83]. To summarize, green materials and fabrication procedures are preferable in the design of the capsules, and their biodegradability is a primary requirement. However, other capsule parameters, such as size, shape, flexibility/rigidity, surface charge, and surface modification, should also be taken into consideration in the design of cancer cell–targeted capsules (Fig. 1).

2.2. Capsule size

The existing approaches to the preparation of multilayer capsules allow easy adapting the particle size in the micrometer and submicrometer ranges. The size of the capsules affects their physicochemical and functional properties, such as the relative surface area and the density of the ligands deposited on the surface, determining the mechanism of the capsule internalization, the rate of their capture by cancer cells, and, hence, the efficiency of their targeted delivery. In addition, the capsule size is an important parameter because it determines their ability to penetrate through tissues and be delivered to the required area.

The size of the multilayer capsules is mainly determined by the dimensions of the templates used for capsule fabrication. To obtain multilayer delivery containers, biocompatible templates are widely used, in particular, microparticles of calcium carbonate or silicon dioxide 3–4 μm in size [84,85]. Particles with an average size within this range are effectively captured by cancer cells [85]. Specifically, the efficiency of the internalization of microcapsules with a size of 3–4 μm has been found to vary from 60 to 95%, depending on the tumor cell line, incubation time, and number of microcapsules per cell (5 and 10) [86]. For example, the rate of the uptake of biodegradable polyelectrolyte microcapsules 3 μm in size by leukemic KU812 cells and normal $CD34^+$ stem cells has been found to range from 70 to 85% [84].

A decrease in the capsule size results in their more effective capture by cells [87]. Moreover, the specificity of the interaction of the particles and the target receptors of cancer cells also increases, which helps to improve the selectivity of the interaction of the particles with cells, as it has been shown for 0.5- and 1.0-μm microcapsules [88]. Larger particles exhibit higher nonspecific binding rates, probably, due to the larger area of contact with the cell membrane. A low rate of nonspecific binding with cells was demonstrated for 0.5-μm particles coated with huA33 monoclonal antibody (mAb), which exhibited an almost fourfold increase in binding compared to controls. The characteristics of binding of 0.3-μm particles with colorectal cancer-derived cells (LIM1215) were found to be similar to those for 1-μm particles. This was attributed to agglomeration of the 0.3-μm particles into aggregates close to 1 μm in size, which was confirmed by fluorescence microscopy data. This suggests that the available surface area of contact with the cell may play a role in the nonspecific binding of the particles. The higher nonspecific binding of larger particles has also been shown in experiments using SW480 colorectal adenocarcinoma cells not expressing the A33 antigen as a negative control (Fig. 2, panels 1 and 2) [88]. Submicron-sized $(PARG/DEXS)_2PARG$ capsules were significantly better internalized by both lung cancer cells and bone marrow–derived macrophages than 2-μm capsules at all capsule densities investigated. The uptake efficiency of ~0.25-μm capsules reached 89.50±0.26% and 76.15±0.77% for lung cancer cells and macrophages, respectively. Apart from the fact that a smaller capsule size is favorable for cellular uptake, this result may have also been accounted for by the difference in the shape between the micrometer- and submicrometer-sized capsules studied [46].

Poly(methacrylic) acid (PMAA) and poly(N-vinylpyrrolidone) (PVPON) hydrogel capsules were found to be significantly decreased in size upon cellular internalization due to local pH decrease. Spherical and discoidal 4-μm capsules were demonstrated to decrease in size by a factor of two upon internalization by human microvascular and breast cancer cells. After internalization by human microvascular cells, the spherical and discoidal capsules were reduced from 4.0±0.5 to 2.8±0.8 μm and from 4.0±0.3 to 1.7±0.8 μm, respectively, in diameter. Internalization by breast cancer cells led to the reduction of the spherical and discoidal capsules from 4.0±0.5 to 2.1±0.5 μm and from 4.0±0.3 to 2.4±0.4 μm, respectively. Thus, the size of the capsules can be altered not only in the course of capsule processing, but also upon interaction with the intracellular microenvironment [89].

2.3. Capsule shape

The effect of capsule shape on cellular uptake is expected to depend on the particle geometry and surface chemistry, as well as the type of target cells. Particles with tailored geometries have received significant attention due to their specific interactions with biological systems [90]. The broad range of available differently shaped templates allows obtaining a variety of replica capsules (Fig. 3, panel 1).

A sphere, however, has only a point contact with a surface at any given time. A flatter morphology increases the area of interaction and, hence, improves the cancer cell targeting

capacity of the multilayer delivery vehicles [91]. Under static conditions, particle shape–dependent cellular association was clearly observed for capsules of thiol-functionalized PMAA/PVPON and mouse fibroblasts, with a particle–cell interaction efficiency of ~90–100% for rods and ~60% for spheres (670 × 670 nm) after 24 h of incubation. A higher degree of association was found for long and short rod-shaped particles with sizes of 7150 × 300 nm and 2020 × 310 nm and was explained by their larger dimensions and, hence, more rapid sedimentation onto the cell surface, as well as a larger surface area interacting with the cells. Under dynamic flow conditions, the cellular association was slightly diminished for rods (~80%) and spheres (~50%) [92]. The data were verified in another study, where phagocytic cells were incubated in the presence of rod-like and spherical capsules 720 × 330 nm or 2250 × 305 nm in size and 670 nm in diameter, respectively. Cellular internalization levels of 90.6%, 96.0%, and 96.8% were observed for spherical capsules, short rod-shaped capsules, and long rod-shaped capsules, respectively [90], which indicated that capsule–cell association and capsule internalization by phagocytic cells were less dependent on the particle shape. The capsule shape, along with the aspect ratio, determines the capsule surface area involved in particle–cell interaction. For example, ~90–100% of hydrogel nanocapsules with a high aspect ratio (80 × 80 × 320 nm in size) prepared by particle replication in non-wetting templates (PRINT) and additionally treated with siRNA and poly-L-lysine (PLL) were found to be internalized by human cervix adenocarcinoma cells at concentrations of up to 20 μg/mL. The use of rod-like hydrogel capsules increased the particle uptake rate; however, it was found to gradually decrease to ~70–80% as the concentration of PLL-coated nanoparticles added to the cells increased [93].

Larger hydrogel capsules (4 μm) consisting of five polymer bilayers that could transform from discoids to oblate ellipsoids upon change in pH, had a hollow structure, and exhibited elasticity were engineered using PMAA and PVPON to confer them the characteristics of erythrocytes in order to use them in a delivery system mimicking red blood cells. Their interaction with three different cell lines, including phagocytic cells, human microvascular endothelial cells, and breast cancer cells, was explored. The discoidal capsules exhibited a 60% lower internalization rate compared to spherical capsules of a similar composition (Fig.6, panel 3) [89]. However, non-spherical particles usually have a higher attachment capacity than their spherical counterparts. During cellular uptake, the cell membrane has to deform after contacts with the particles and then wrap the particles to eventually engulf them [94]. Bowl-like hemispherical multilayer PAH/PSS microcapsules prepared by osmotic-induced invagination of their spherical counterparts in a concentrated polyelectrolyte solution tended to attach to the cell membranes on the bend side and could be enwrapped by the membranes of smooth muscle cells, which led to a faster uptake rate and larger accumulation inside cells compared to the spherical capsules. Moreover, over 80% of cells internalized the bowl-like capsules, whereas this proportion was only about 56% for the spherical ones, which indicates that the bowl-like shape is more favorable for cellular internalization than the spherical one. In the case of bowl-shaped microcapsules, the uptake was mediated by clathrin- and caveola-mediated endocytosis, whereas in the case of spherical microcapsules, clathrin-mediated endocytosis and the cytoskeleton were involved in the internalization process. With a similar diameter (approximately 2 μm), the volume of bowl-like capsules was smaller than that of spherical capsules, which means that fewer cells were required for particle internalization [95].

Similarly shaped 2-μm hemispherical hydrogel microcapsules of hydrogen-bonded PVPON/tannic acid (TA) were observed to be successfully internalized by phagocytizing cells (human monocytic leukemia cells differentiated into macrophages), with the uptake two times more efficient compared to spherical and cubical microcapsules of the same composition (Fig. 4, panels 1, 2) [68]. Disc-shaped polyurethane microcapsules fabricated by the adsorption and crosslinking method on templates with the corresponding shapes in an organic solvent and incubated with mouse macrophages and human hepatocellular carcinoma cells exhibited an enhanced cellular uptake and internalization with a faster rate for both types of cells. The number of cells interacting with the disc-shaped capsules within 12 h was more than twice as large as in the case of spherical microcapsules. In this study, macrophages displayed a higher capsule uptake rate [94].

2.4. Capsule rigidity

The multilayer assembly determines both the capsule processing properties (such as the duration of the fabrication, number of fabrication cycles, and scalability) and the physicochemical properties of multilayer films constituting the capsule shell (such as the thickness, homogeneity, and inter- and intra-layer film organization), which are so selected as to increase the application-specific performance. An increased number of polyelectrolyte layers deposited via layer-by-layer microcapsule assembly helps to enhance the microcapsule stiffness but increases the variation of the absolute stiffness values within the microcapsule batches [77]. Saving the template core after deposition of the polyelectrolyte layers results in the formation of rigid core/shell capsules with a solid internal structure [96]. The internal structure of the microcapsules is tuned by template removal by dissolving it with a specific solvent. Complete dissolution of the template leads to a formation of hollow and soft structures with aqueous contents. Additional strengthening of the shell is ensured by cross-linking the polymer pairs constituting the shell. Hence, the microcapsules with strengthened shell were assembled from PMAA/PVPON and subsequently cross-linked with 1-ethyl-3-(3-(dimethylamino)-propyl)carbodiimide hydrochloride (EDC) and ethylenediamine (EDA) hydrogel film stable for more than 140 h under deteriorating acidity conditions [40]. Most polymers used in microcapsule shell fabrication are decorated with primary amine or carboxyl functional groups, which makes the carbodiimide EDC an attractive zero-length linker [32]. However, other low-molecular-weight shell strengthening

components , such as tetraethoxysilane (TEOS), calcium ions, and cystamine, are also extensively used [22,25,30,97].

Hollow capsules are tightened and deformed during cellular internalization, depending on their stiffness characteristics [77]. The capsule rigidity significantly affects internalization by cancer cells, with a greater uptake rate of rigid or strengthened particles than soft ones (Fig. 2, panel 3). Stiff capsules consisting of a silicon particle template coated with five bilayers of PMAA/PVPON hydrogel were found to be taken up by breast cancer cells at a three- and seven-fold increased rates compared to hydrogel capsules of the same shape and a similar size in the cases of spherical and discoid templates, respectively [89]. Soft polysaccharide capsules obtained via continuous assembly of polymers on silica templates using atom transfer radical polymerization (ATRP), with methacrylated hyaluronic acid (HA) serving as a macro-crosslinker, had a stiffness (γ) of 7.5 mN m^{-1} and a higher cell surface binding and cellular association rates compared to stiffer capsules with γ of 17.6–28.9 mN m^{-1}. The uptake of HA capsules was shown to be a stiffness-dependent process, the cellular internalization rate and the total amount of accumulated capsules decreasing with increasing capsule stiffness. Nevertheless, regardless of the stiffness, all internalized capsules were deformed and located in the lysosomes of the human cervix adenocarcinoma cells [98]. The further fate of the capsules after internalization was also proved to be affected by their rigidity. The uptake was monitored in situ by analyzing individual particle trajectories, including the progress of endocytosis, on the basis of local pH measurements around each particle. Evidence was presented that soft particles with a low stiffness were transported to lysosomes faster than stiffer ones [77]. The stiffness of the nondegradable PAH/PSS and degradable DEXS/PARG capsules regulated by the number of polyelectrolyte layers influenced their internalization by human cervix adenocarcinoma cells. Both types of the capsules were internalized by the cells in similar ways and were ultimately located in lysosomes. However, the time of acidification of PSS/PAH capsules increased linearly with capsule stiffness independently of the particle size, whereas no such dependence was found for DEXS/PARG capsules. Thus, the uptake itself and the subsequent endosomal trafficking were found to strongly depend on the stiffness of the particle, whereas further processing and acidification were mainly governed by the capsule building-block chemistry [77]. To further illustrate the stiffness-dependent cellular processing behavior and investigate the important role of capsule stiffness in their biological performance, numerous cell lines and different capsules should be explored [98].

2.5. Capsule surface charge

The multilayering strategy of capsule fabrication allows tuning the surface properties of the particles during their fabrication through addition of polymers, including polyelectrolytes bearing charged functional groups, such as amine (CHI [26,27,38,99], PAH [10,24,37,100], PLL [29,32], PARG [21,22,42], and poly(diallyldimethylammonium chloride) [27]), sulfonate/sulfate (PSS [24,37,100] and DEXS [21]), carboxyl (HA [99], ALG [38,42], polyglutamic acid [29], polyacrylic acid (PAA) and its derivatives [28,101], and PMAA [59,102]) groups, which are subsequently exposed on the capsule surface.

The role of the capsule surface charge, other surface properties, and size in particle–cell interaction has been studied in detail. For example, positively charged (+60 to +70 mV) 60- to 80-nm amine-containing PLL particles were more readily taken up by HEK293 cells than negatively charged ones carboxylated with polyglutamic acid (–40 to –45 mV) in a serum-free medium. The opposite charges of the PLL-coated capsule shell and the cell membrane resulted in electrostatic-driven interaction, which was significantly decreased in the presence of fetal bovine serum (FBS) in the incubation medium [103]. Because the capsule size determines the relative surface area, the capsule dimensions directly affect the distribution of the functional groups of polyelectrolytes on the particle surface and the surface charge density. All of these factors together affect the association and subsequent internalization of the capsules by cancer cells. The dynamics of the interaction of positively charged PARG-coated 5-μm polyelectrolyte microcapsules with HEK293 cells was characterized by initial accumulation reaching a plateau within 5 h at microcapsule-to-cell ratios of 5 and 10. Estimation of the kinetics of cellular internalization rate (the percentage of microcapsule uptake) for microcapsules negatively charged due to the final layer of dextran showed a peak after 4–5 h of incubation at microcapsule-to-cell ratios of 5 and 10. A gradual decrease in the adsorption of negatively charged capsules was supposed to be caused by a massive microcarrier adsorption [96].

The size of the surface ligand may also affect the internalization efficiency. This has been shown, e.g., for positively charged (40±1 mV) mesoporous silica nanocapsules (169±3 nm in size) labeled with fluorescein isothiocyanate (FITC) and functionalized with CHI, which were poorly internalized by mouse fibroblasts because the particles tended to form large aggregates outside the cell membrane or over the cells. In contrast, FITC-fluorescent aminopropyl-TEOS silica nanoparticles bearing NH_2 surface functional groups (126±2 nm), which had a small positive charge (+9.7±0.8 mV), were also internalized by the cells (~79% according to flow cytometry data) [99]. Nanocapsules engineered from hydroxyethyl starch using the emulsion technique were characterized by a negative surface charge (–27 mV at pH 7.0) and very low internalization efficiency by human cervix adenocarcinoma and epithelial lung carcinoma cells [104] due to electrostatic repulsion and occasional chaotic particle–cell association. Surface modification with electrically neutral polymers, e.g., polyethyleneglycol (PEG) or its non-functionalized derivatives leads to the formation of a slightly negative (close to neutral) particle surface charge and results in the stealth effect preventing particle–cell association. For example, PEGylated mesoporous silica capsules with a slightly negative charge (~ –8 mV) exhibited negligible association with human cervix adenocarcinoma cells and phagocytic cells, with an internalization efficiency of less than 10% [105].

When multilayer capsules interact with physiological environment, they are opsonized, which results in alteration of the capsule surface charge [95]. In particular, the adsorption of proteins was found to lead to neutralization of the negative (about –40 mV) surface charge of soft PMAA capsules and rigid core/shell silica–PMAA capsules. However, surface charge neutralization up to about –30 mV was observed in the case of hollow capsules in FBS-containing medium, human serum, and plasma (Fig. 3, panels 2 and 3). The charge-quenching effect of the components of the physiological environment depended on the total amount of protein contained in the incubation medium. A higher protein content in the capsule microenvironment was likely to result in a denser surface coating of the particles with proteins and lead to different extents of inhibition of their uptake by cancer cells [102]. Biosimulation studies showed that multilayer polyelectrolyte architectures with a neutral PEGylated surface exhibited lower opsonization with human serum albumin (HSA), fibrinogen, and FBS compared to non-PEGylated samples with protein-resistant properties [106]. Thus, occurrence of charged components of serum on the capsule surface leads to indicative changes in surface properties of both positively and negatively charged multilayer capsules towards surface neutralization, which results in weaker particle–cell interaction.

3. Surface modification of the polymeric multilayer capsules for cancer cell targeting

3.1. Functionalization with full-size antibodies and their fragments

To enhance the selectivity and targeted interaction of multilayer capsules with cancer cells and enable targeted delivery, biofunctionalization of their surface is performed. This modification ensures the opportunity of specific capsule adsorption through ligand–receptor interaction on the cell membrane where target molecules are located. Passively targeted capsules are internalized by most types of cells; however, in the case of delivery to cancer cells, it is reasonable to ensure focused interaction with specific cell domains or substructures representing tumor-specific surface markers or receptors. The most common way to direct the capsules to cellular targets is to use highly specific capture molecules, such as immunoglobulin G (IgG) antibodies (Fig. 5). mAbs, as well as their capture fragments, are now extensively employed as cancer cell–targeting molecular vectors recognizing highly specific extracellular homotypic moieties of cancer cells [8,82,107].

Full-size IgG mAbs are characterized by an average molecular weight of ~150 kDa and a hydrodynamic diameter of ~9 nm with average single-molecule dimensions of 14.5 × 8.5 × 4.0 nm [108–110]. A variety of exposed functional groups, such as amine and carboxyl ones, in the mAb structure allows using bioconjugation approaches for functionalization of the capsule surface [111–113]. Prior to biofunctionalization, the surface of the multilayer capsules requires chemical modification to expose specific functional groups (carboxyl, amine, etc.) for further bioconjugation with mAbs or their fragments. The possible approaches to mAb immobilization on the capsule surface include electrostatic adsorption, covalent coupling, and non-covalent protein–protein binding [11,45,114] (Fig. 5).

Passive electrostatic adsorption yields a non-oriented layer of negatively charged mAbs on the positively charged capsule surface coated, e.g., with protamine sulfate or PAH. Although the method is easy and quick, electrostatic attachment is less strong than covalent coupling and also requires blocking unspecific binding sites with BSA [101,115]. Direct covalent coupling of mAbs via carbodiimide cross-linking to the soft carboxylated capsules coated with PAA ensures strong binding of the NH_2 groups of mAb molecules to the microcapsule surface and more specific attachment of the capsules to breast cancer cells [11]. Carbodiimide surface activation ensures the preservation of dispersity of the resultant microcapsules [11]; however, this approach results in non-oriented mAb deposition hiding active sites of the mAbs and making them partly inaccessible for ligand–receptor interaction [116]. Carbodiimide coupling allows rigid microcapsules with solid polystyrene cores to be effectively functionalized with mAbs against prostate-specific antigen (PSA) and enables PSA sensing with the use of these capsules [117]. Click-chemistry reactions using azide-functionalized mAbs, alkyne-modified capsules, and a chelated Cu(I) catalyst have also been successfully employed in biofunctionalization of the capsule surface and delivery to colon cancer cells [59]. Direct streptavidin/biotin linking ensures non-oriented deposition of antibody molecules in the course of surface modification of multilayer capsules [115].

After mAb coupling to the capsule surface, the bioconjugation is stopped by addition of TRIS, hydroxylamine, or glycine in the case of carbodiimide-based coupling, and the capsule is back-coated with biopolymers [11,45,118]. The chemical sense of quenching of the mAb bioconjugation is blocking the pre-activated surface sites free of mAb molecules. Capsule back-coating with BSA enhanced the particle colloidal stability and dispersity [119]. However, the mAb-conjugated capsules can be back-coated with HSA, which is actively used in particle engineering due to the minimal cytotoxicity and good biocompatibility as a structural component for capsule shell formation [120,121]. From the pharmacological point of view, quenching and back-coating prevent side effects of the capsule delivery systems prior to their contact with physiological environment. The use of HSA is advantageous because it is a major constituent of the human serum and its main component is involved in capsule opsonization during their interaction with physiological environment [120,122]. Human serum can be also used as a source of native biocompatible materials for capsule back-coating [59].

The effectiveness of cell targeting can be significantly improved by optimizing the arrangement of the targeting ligands on the capsule surface. The orientation, density, and flexibility of the targeting ligand on the particle surface are crucial parameters for optimization of the cell binding [123]. For example, multilayer DEXS/PARG microcapsules were assembled and functionalized with mAbs via streptavidin using PLL-PEG-biotin and subsequently coupled with biotinylated

protein G for further immobilization of mAbs [124]. Protein A can be also covalently attached to carboxylated $(PAH/PAA)_2$ capsules by carbodiimide surface activation of the carboxylic acid groups in the terminating PAA layer. Afterwards, antibodies are immobilized on the capsules coated with protein A in an oriented manner due to the high affinity of protein A for the Fc domain of the antibody [45,125].

However, the antibody structure can be customized to enhance the oriented coupling and antigen binding capacity of the biofunctionalized capsules; e.g., bispecific Abs (bsAbs) that contain dual antigen-binding sites can be used. In some studies, bsAbs against a specific protein and a component of the capsule surface are used for better interaction and specific orientation of the antibodies [126]. For example, hollow spherical and rod-shaped PEG capsules with tunable aspect ratios were synthesized and subsequently functionalized in an oriented manner with bsAbs (~54 kDa) that had dual specificities for PEG and epidermal growth factor receptor (EGFR). bsAb-functionalized PEG capsules exhibited a >90% specific cellular association with EGFR-positive MDA-MB-468 human breast cancer cells and negligible association with both control cell lines (EGFR-negative CHO-K1 Chinese hamster ovary cells and RAW 264.7 murine macrophages) after incubation for 5 h [82,126]. The size (≥0.5–1 μm) and surface area characteristics of the multilayer capsules provide an advantage in their surface biofunctionalization via bioconjugation, which allows successful implementation of non-oriented, random coupling to target the capsules to cancer molecular markers. Non-oriented coupling is more likely to result in a larger occupation of the surface with mAb molecules. Given equal probabilities of different mAb orientations on the capsule surface, at least 50% of the molecules deposited should expose their active sites for further selective interaction with molecular targets. For example, carbodiimide conjugation of mAbs to the surface of 5-μm multilayer capsules will result in a coupling efficiency of 3×10^6 mAb molecules per microcapsule, with at least 1.5×10^6 mAbs sterically accessible. The click chemistry approach provides a surface coverage with mAbs of $7.5\pm0.7\times10^4$ mAb molecules per 2-μm capsule, which is assumed to correspond to 3.8×10^4 mAb molecules with available binding sites [59]. In the case of oriented linking of the mAbs to 6- and 3-μm capsules, the coupling efficiency is 4×10^5 and 1×10^5 mAb molecules per capsule [45,112]. Therefore, oriented conjugation of mAbs with capsules of smaller sizes comparable with routinely available nanoparticles (≤0.5 μm) is a more promising approach to surface biofunctionalization. The use of non-oriented linking techniques in this case provides less effective vectorization due to the decreased total percentage of appropriately deposited mAb molecules. Thus, the surface area and particle sizes are among the factors that should be taken into consideration in choosing the capsule mAb-functionalization strategy. The ligand size is also an important factor to be considered in biofunctionalization and cancer cell targeting of the capsules. Specifically, full-sized mAbs are optimal vector molecules because their affinity for specific antigens is as high as 10^{-9} M and their molecular dimensions are likely to prevent their shielding with back-coating agents or opsonization molecules. However, when an mAb is coupled to the capsule surface, its affinity for the ligand may alter, although this situation can be overcome by choosing an appropriate ligand density and orientation at the capsule surface [125].

3.2. Functionalization with peptides, proteins, hyaluronic acid or nucleic acids

The capsule surface can be functionalized not only with mAbs, but also with other ligands that possess affinity for some cell surface molecules or structures (Fig. 5). The effect of this functionalization may consist of either activation or suppression of the immune response, as well as activation of a specific type of phagocytosis or phagocytic cells. The use of peptides recognizing receptors on the surface of dendritic cells, macrophages, and cancer cells has been shown to be an effective method for delivery of therapeutic agents [127–129]. However, under physiological conditions, antibodies are more efficient than peptides [130]. The balance between the level of degradable microspheres and their functionalization can modulate the activity of microspheres and their effectiveness. The time of degradation affects the level of specific stimulation of cells [131]. As with mAbs, not only does the surface modification affect the cell uptake kinetics, but also the ultimate extent of internalization is determined by the cell type and size. The peptide modification significantly promotes the uptake of 700-nm hydrogels by hepsin-positive MCF-7 cells due to ligand–receptor recognition but has a negligible effect on the uptake of 2-μm PMAA hydrogel capsules. The selectivity of 700-nm IPLVVPL-PMAA hydrogel cubes for hepsin-overexpressing tumor cells is further confirmed by a three- to tenfold higher rate of particle internalization by hepsin-positive MCF-7 and SK-OV-3 cells compared to hepsin-negative PC-3 cells [56]. The effectiveness of the antibacterial peptide melittin attached to the surface of poly(ethylene glycol) diacrylate hydrogel microspheres was similar to the effectiveness of the same recombinant peptide released from microspheres [132].

Folate receptors are widely expressed on the surface of cancer cells, especially at the last stages of tumor formation. Therefore, folate receptors represent one more target on the cancer cell surface against which multilayer capsules can be vectored. Bioconjugation with folic acid performed using carbodiimide chemistry onto amine pre-functionalized particle surface results in a more specific interaction of the particles with the surface of HeLa and Jurkat cells [133]. Exposure of specific enzymes on the surface of microcapsules allows the internalization to be improved for specific types of tissues. Neuraminidase cleaves N-acetyl neuraminic acid residues of glycoproteins and targets the sialic acid component of the glycocalyx on the cell membrane, which makes it one of the possible vectors for functionalizing multilayer capsules to enhance capsule uptake by the cells [134]. Hyaluronidase, a tetramer with a molecular weight of 60 kDa and molecule size of 6 nm, which catalyzes the hydrolysis of the b1/4 glycosidic bond in HA and chondroitin sulfate, can be used for

improvement of capsule delivery to cancer cells. Hyaluronidase degrades HA molecules into smaller fragments and loosens the tumor stroma, which ensures more effective penetration of the delivery systems into tumors. Rigid core/shell silica nanoparticle/PAH/hyaluronidase nanocapsules with exposed hyaluronidase that contained the drug cisplatin were introduced into tumors, which resulted in a significant enhancement the tumor volume reduction with silica nanoparticle-immobilized hyaluronidase compared to capsules without non-immobilized hyaluronidase [135]. On the other hand, hyaluronidase can promote tumor progress and invasion through depolymerization of HA, because the depolymerization products can induce angiogenesis in the tumor. HA and its receptors, such as CD44, are expressed by cancer cells. The CD44 antigen is normally expressed on the cell surface of hematopoietic cells. This marker also has an HA-binding capacity. Variations of the CD44 expression have been reported for some breast and prostate cancer stem cells, head and neck squamous-cell carcinoma, and other types of cancer. Functionalization of microcapsules with HA can target them to CD44-overexpressing cells. By varying the ratio between HA and PEG, particles can be obtained that efficiently recognize $CD44^+$ cells but display a low nonspecific binding to $CD44^-$ cells [136]. The specificity of HA for $CD44^+$ cells is also retained in capsules consisting of the HA polymer. HA capsules are poorly absorbed (<22%) by HeLa, BT474, RAW0020264.7, and THP-1 cells but exhibit a high targeting specificity for the CD44-overexpressing MDA-MB-231 cells [105].

Due to the charged surface, electrostatically driven adsorption of nucleic acids onto the capsules is possible [41]. Nucleic acids are used for recognition and specific binding to proteins and other targets due to their small size, low immunogenicity, and high specificity. Aptamers with EGFR-specific RNA based on hollow gold nanospheres have been used to image and capture tumor cells and have been found effective ligand for cancer cell targeting [137]. TLR3 ligand polyriboinosinic acid-polyribocytidylic acid (poly(I:C)) mimicking double-stranded RNA can also be used to activate innate immunity through interaction and activation of TLR3 followed by the launch of various signaling pathways [58].

3.3. Interactions of the capsules with the constituents of biological fluids

Interaction of the capsules with external fluids in the human body influences the effectiveness of their delivery to the tumor growth areas. The capsules are supposed to interact with cell, plasma, and serum proteins. In this case, the capsule surface is opsonized and a protein corona is formed on the surface of the capsules. The formation of the protein corona out of adsorption proteins is a dynamic process that has several phases. First, a tightly, irreversibly bound layer of proteins is directly adsorbed onto the particle surface; then, an intermediate layer is formed from proteins that are not directly attached to the surface but are still irreversibly bound and, hence, are part of the inner “hard” protein corona; and after that, an outer protein layer, the “soft” protein corona consisting of reversibly bound components is attached [138]. Nonspecific adsorption of biological molecules on the surface of particle-based delivery systems can yield different results. First, it can be opsonized with complement system components and then nonspecifically taken up by macrophages [139]. Second, in the case of functionalization of the surface of microparticles with targeting antibodies or other molecules, plasma components may reduce the effectiveness of antibody targeting by shielding them with nonspecific molecules. Absorption of proteins from human plasma on the particles has been shown to decrease the particle binding to the cell membrane, increase the residence time of the particles in early endosomes, and reduce the amount of internalized particles within the first hours of cell exposure to the particles [86,102,120].

Adsorbed proteins can alter the capsule targeting capacity as they enter biological environments. A dramatic decrease in the specific association rate (from ~70% to ~7%) was shown for polymer-coated silica particles functionalized with low-molecular-weight antibody-mimetic ligands upon opsonization with serum proteins, whereas opsonization with HSA alone enhanced the specific association of the functionalized particles with SK-OV-3 human ovary cancer cells (to ~90%) [140]. In another case, coating of micron and submicron capsules with a HSA/TA shell increased the colloidal stability of the capsules in human serum [121]. Nonspecific interaction between the capsules coated with HA and cells was significantly reduced in the presence of absorbed proteins derived from human serum [136]. On the other hand, adsorption of proteins may promote the delivery of capsules and their uptake by the target cells or do not affect these processes. Opsonization of mAb-biofunctionalized PMAA capsules enhanced their binding to cancer cells. However, the targeting capacity of rigid capsules was even higher. Analysis of the cell-membrane binding of the mAb-functionalized soft and rigid capsules targeted to colon carcinoma cells confirmed that the specific binding driven by mAb–antigen interactions was the same in the absence and presence of the “hard” protein corona layer [59]. The targeting specificity of metal–phenolic capsules was enhanced due to the formation of a layer of adsorbed proteins [136]. Low-fouling zwitterion-coated particles are characterized by weaker interaction with irreversibly bound proteins, and only a “soft” protein corona is formed on these particles [138].

The capsules may interact not only with proteins in physiological liquids. Apart from plasma and serum proteins, the microcarriers may be covered with anazotic molecules, such as glucose, fatty acids, phospholipids, and cholesterol. They affect the interaction of the particles with cells, but this effect has not been investigated in detail [141]. In the case of intravenous injection of microcapsules, they interact with whole blood components: red blood cells, white blood cells, plasma, and platelets. The microcapsules can also interact with endothelial cells in vessel walls. The microparticles interaction with all groups of cells that are present in the blood are also poorly explored. Phagocytosis of fluorescent microspheres has been analyzed using different human cells, including

differentiated THP-1 cells and blood monocytes. The microspheres were partly covered with BSA. The microparticles were efficiently internalized in a non-opsonized form and in a dose-dependent manner by both cell types [142]. Enrichment of the biomolecule corona with specific proteins correlates with binding to specific cell types. Zwitterionic poly(2-methacryloyloxyethyl phosphorylcholine)-based replica particles representing capsules displayed reduced association both with cells and with serum proteins compared to mesoporous silica-based particles used as templates for the assembly of the polymeric shell. Nonspecific interaction of the particles with immune cells and their cellular uptake are independent of the adsorption of serum proteins in general, but the particles should exhibit weak association to specific proteins [143]. In the case of uptake of polyelectrolyte capsules by peripheral blood mononuclear cells, there is no immune response, and the expressions of TNF-α and IL-6 are not increased [86]. However, in the case of interaction of immune cells (peripheral blood mononuclear cells) with polystyrene latex beads and their subsequent co-culturing with cancer cells (the HT-29 human colorectal adenocarcinoma or RKO human colon carcinoma cell line), the amounts of three pro-inflammatory cytokines, TNF-α, IL-1β, and IL-6, decrease, while those of the anti-inflammatory IL-10 and IL-1ra remain unchanged [144]. The presence of PEG molecules on the capsule surface may prevent the capsule uptake by phagocytic cells [145,146]. However, the presence of targeting molecules on top of the PEG coating may enhance the capsule interaction with phagocytic cells, although association with monocytes and granulocytes is not changed significantly after functionalization of PEG-110 capsules with bsAbs. These results indicate that bsAb modification does not influence the stealth properties of PEG-110-particles functionalized with bsAbs *ex vivo* [126]. According to the simulation study, the particles can collide with red blood cells, and this affects their distribution. Elongated particles are more likely to further interact with the vessel wall than flat and spherical particles are. Once the contacts with the wall are formed, the likelihood of firm adhesion is greater for disk-like particles, smaller for elongated particles, and even smaller for microspheres [147].

4. Cancer cell targeting, internalization, and uptake of polymeric multilayer capsules

4.1. Relationship between the cancer cell type and capsule design

Surface biofunctionalization of capsules with mAbs against a given molecular cancer target will enhance the specificity of the capsule delivery and thereby improve drug release by localizing the delivery systems in a close contact to the target cells. Human epidermal growth factor receptor 2 (HER2, ERBB2) is one of the classical cancer molecular markers. Capsules conjugated with Trastuzumab, a humanized mAb targeting the extracellular domain of HER2, exhibit sufficiently sensitive and specific antibody-mediated binding with live cancer cells, e.g., SK-BR-3, which demonstrates their potential as prospective cancer cell–targeting agents [11]. EGFR is another widespread cancer marker. The microcapsules modified with anti-EGFR mAbs or anti-EGFR bsAbs can effectively recognize specific cells (Fig. 7, panels 1, 2) [112,126]. MDA-MB-468 human breast cancer cells are sometimes used as a model cell line with a high rate of EGFR expression. It has been shown that bsAb-functionalized PEGylated capsules have a specificity of association with EGFR-positive cells of >90%, their association with control cell lines (EGFR-negative CHO-K1 Chinese hamster ovary cells and RAW 264.7 murine macrophages) being negligible [82]. Ab-functionalization of the capsule surface enhances the specific attachment of the capsules to cancer cells, but both this process and further uptake of the capsules depend on their physicochemical properties. Summary information about the influence of individual characteristics on the interaction and further internalization of capsule-based microcarriers with various model cancer cell lines is presented in Table 1. Negatively charged micrometer-sized capsules are frequently used in capsule–cell interaction studies. It has been shown that positively charged and neutral capsules sometimes less strongly interact with the cell membrane [96].

The HeLa human cervix adenocarcinoma cell line is the most popular model for investigating capsule targeting towards cancer cells. The most common type of capsules used in these studies has a soft shell structure [23,26,77,85,98,104,105,148]. In the case of nonspecific interaction, uptake of differently sized (appr. from 0.3 to 5 μm) capsules was observed (Fig. 6, panels 1–4), and internalized capsules were detected in lysosomes, as shown in Fig. 6 (panel 2). Folic acid attached to the capsule or microsphere surface enables the capsule interaction with cancer cells in a targeted manner, with subsequent internalization mediated by the folate receptor FRα [104,133]. Functionalization with a peptide ligand of the CD44 receptor induces CD44-receptor-mediated endocytosis [26]. Human breast adenocarcinoma lines, including MCF-7, MDA-MB-231, MDA-MB-468, BT474, and SKBR-3, are widely used as models for investigating targeting and internalization to breast cancer cells [38,56,85,105,114,126,149]. Antibodies against molecules or receptors overexpressed in these cancer cells (EGFR, CEA, HA, etc.) have been used as targeting molecules in the case of breast cancer cell lines. Spherically shaped capsules are most common; however, cubical and rod-shaped capsules have also appeared to be effective for cell surface interaction and further uptake [56,82]. Both soft and rigid spherical microcarriers about 3–4 μm in diameter are internalized by human adenocarcinoma cells via lipid raft–mediated macropinocytosis, whereas the same particles in the case of human lung adenocarcinoma are taken up by phagocytosis [149]. The LIM1899 human colon adenocarcinoma and A549 human lung adenocarcinoma cell lines have also served as model cell lines in several capsule-uptake studies [59,77,88,149,150]. The issue of efficient cancer cell targeting still represents a major challenge in designing the delivery systems and providing their functionality. In particular, the characteristics of particle–cell interaction in these models are to be considered, but data on this subject are scarce.

4.2. Delivery of the targeted capsules to the tumor growth area

Tumor microenvironment plays an important role in tumor growth and development. It consists of immune cells, blood vessels, fibroblasts, and extracellular matrix surrounding cancer cells. Interaction between the components involving signal molecules can affect the tumor. The standard methods for studying this influence are not completely harmonized and disregard the complexity of the tumor microenviroment [151,152]. The tumor microenvironment also affects the therapeutic response and, hence, should be taken into account when choosing the tumor treatment strategy. One of the key components of the tumor microenvironment is tumor-associated macrophages. They play an important role in the disease progression. The role of interaction between mononuclear cells and microcarriers has been only partly investigated [144]. Because of the cells' capacity for phagocytosis, all capsules without targeting are intensely absorbed by monocyte–macrophage cells [77,94,105,148]. Opsonization of carriers with serum proteins leads to a decrease in the cellular uptake of the particles. The inhibition of the particle uptake is stronger in the case of THP-1 and HeLa compared to dTHP-1 cells. The cellular uptake mechanisms of monocytic and epithelial cell lines are different [102]. U937 monocytic cells intensely interacts with negatively charged capsules and particles [96]. The carriers functionalized with anti-EGFR bsAbs display a highly specific association with EGFR-positive human breast cancer cells and negligible association with control murine macrophages [82]. It has been shown that multifunctional complexes containing anti-HER2 mAbs, lipopolysaccharide, and/or mannose have a high capacity for binding HER2-positive cancer cells, causing the expression of IL-1 and attachment of activated monocytes to HER2-positive cells [153]. Hence, according to experimental results, the most effective approach to capsule functionalization is designing the capsules targeted to both cancer cells themselves and the tumor microenvironment.

One of the possible strategies ensuring capsule targeting to tumors is the use of cell–capsule delivery platforms, in particular, human mesenchymal stem cells loaded with polymer capsules [154,155]. Mesenchymal stem cells exhibit a high capsule internalization efficacy and are characterized by tropism to the tumor microenvironment, which makes them attractive delivery vehicles for capsule targeting to the tumor growth area [156].

4.3. Intracellular fate and internalization pathways of the cancer cell–targeted capsules

Capsule internalization noticeably depends on its properties. For example, at the first stage of interaction of capsules with cells, nonspecific interaction occurs due to electrostatic forces. The ζ-potential of the cellular surface is mostly negative, about –10 to –30 mV. Therefore, capsules with a positive ζ-potential nonspecifically interact with cells [96]. This type of capsules is characterized by an initial fast increase in the interaction rate, after which, without a special initiation signal, the rate becomes lower. In the case of phagocytosis, cytoskeleton components are involved at the next stage, and a phagocytic cup is formed to fix capsules at the plasma membrane. The capsules are co-localized with lipid rafts, which facilitates further cytosolic invagination. This process activates the cell to initiate macropinocytosis. Multilayer polyelectrolyte capsules 3–4 μm in diameter are sorted to heterophagolysosomes and finally localized in the perinuclear cytoplasm [114,149]. Softer microcarriers can be easily deformed and internalized. Therefore, cellular uptake of soft capsules is more effective than that of rigid particles, and biodegradable capsules are more effectively internalized than non-biodegradable ones, which have a more rigid structure [77,85,150]. Small capsules often have a slightly more flexible structure, and they are more prone to be taken up [82]. After internalization, the capsules are located in late endosomes or lysosomes [150]. As a result of interaction with lysosomal enzymes, the contents of the capsules can be detected in both cytoplasm and nucleus [38]. The capsules functionalized with the peptide recognizing the CD44 receptor are efficiently internalized by HeLa cells via the CD44-receptor-mediated endocytosis [26]. Functionalization of the capsule surface with IgG may also affect the ways of nonspecific capsule internalization. The breast epithelial cell line MCF-10A, which exhibited different mechanisms of internalization, could not take up IgG-coated particles by either macropinocytosis or dynamin-dependent endocytosis, whereas SKBR-3 cells internalized all types of microparticles by macropinocytosis, which was possibly due to variation of the accessibility of antigen sites on the cell surface [114,157]. Close contact between the phagocytic cell and the capsule is a prerequisite for efficient phagocytosis, which suggests that therapeutic antibodies should target small antigens [158].

4.4. Biodistribution and tumor targeting of the capsules *in vivo*

The biodistribution of targeted capsules containing drugs after administration to mice has not been sufficiently studied yet. A series of studies were aimed at tracing further biodistribution of drug-loaded capsules after injection directly into the tumor. The biodistribution of capsules strongly depends on their size [121]. Micrometer-sized capsules mostly accumulate in lungs 10 min after injection. After that, these microcapsules can be successfully internalized by lung macrophages and epithelial cells. Submicrometric particles pass through lungs and accumulate in the liver and spleen. Other researches dealt with the effect of functionalized capsules on tumor cells. There are few data on the effectiveness of functionalized capsules administered intravenously or intramuscularly and on their biodistribution in animal models. Experiments with intratumoral injection of doxorubicin-loaded functionalized BSA–gel capsules in mouse models have shown predominant accumulation of the carriers in tumor tissues, with insufficient amounts found in healthy organs, including the heart, liver, lung, spleen, and kidney, which indicates that the systemic toxicity of doxorubicin is negligible in this case [38]. Novel drug-loaded thermo-sensitive hydrogel rod-shaped nanoparticles based on surfactant polymers provide a high drug-loading capacity, steady drug release, and prolonged drug retention within the tumor [159]. The efficiency of capsule-based delivery of anticancer drugs may be decreased by vascular leaks at the surface/periphery of the tumor [160]. Folic acid–conjugated capsules with an encapsulated caspase 3 activator specifically deliver the drug to colon cancer cells and display a high therapeutic efficacy and weak side effects [161]. Biofunctionalization of the capsules with bsAbs does not

significantly improve tumor targeting in mice, but it does not cause a significant increase in the liver or spleen accumulation *in vivo* either (Fig. 7) [126]. In a mouse model of lung cancer, the therapeutic efficacy of capsule delivery systems has also been shown to be affected by the tumor microenvironment. The capsules were also internalized by liver cells with a high efficiency [46].

5. Conclusions and future prospects

Multilayer capsules represent a promising delivery platform that can be effectively adapted for cancer cell targeting. The possibility of wide use of biodegradable and biocompatible structural components in capsule engineering enables the development of safe and effective delivery systems. The capsule size, shape, rigidity, and surface properties can be tuned to enable more effective delivery and capsule–cell interactions. Smaller-sized capsules may provide more effective delivery due to a higher specificity of capsule–cell interaction. However, in this case, their capacity characteristics, including surface area and volume, are reduced compared to that of large capsules (≥0.5–1 μm). The capsule geometry directly affects their cellular uptake; the higher surface area of the capsules enables more sites of contact at the cell membrane and, hence, more effective uptake of the capsules with tailored dimensions. The shape tortuosity has been shown to facilitate capsule uptake, as it was observed for discoid-like capsules. Rigid capsules with the core/shell structure are more likely to be taken up and subsequently internalized by cancer cells, whereas hollow shell capsules contact with the cell membrane more effectively, their soft structure enabling their deformation during delivery and their penetration through tight spaces within tumor blood vessels, which is advantageous for targeting the cancer cells and tumor growth area, respectively. Capsule surface properties, including the surface charge, are determined by specific functional groups and influence capsule–cell association. Surface biofunctionalization additionally improves the capsule biocompatibility and enables capsule vectorization towards cancer cells and molecular targets expressed by them. To date, several vector molecules have been explored as vectorization ligands for cancer cell–targeted delivery, including folic acid, hepsin, HA, hyaluronidase, and mAbs. These last are the most promising ligands due to highly specific antibody–antigen interaction. However, despite the variety of techniques for oriented and non-oriented mAb conjugation, this approach to capsule functionalization is still challenging because the problems of preserving mAb affinity after bioconjugation and their optimal surface orientation have not been solved completely. The phenomena of opsonization and interaction of mAb-functionalized capsules with cellular and molecular blood components are poorly explored. There is information about ways of internalization of capsules into phagocytic cells, but the data about the mechanisms of cancer cell uptake are scarce. Obtaining these data is important because different cells may employ different types of internalization, which affects the final arrangement of the drug-loaded capsules in the intracellular compartments. The structure of tumor microenvironment plays an important role. The capsules can nonspecifically interact with all cellular components of this environment: phagocytic immune cells, endothelial cells of blood vessels, fibroblasts, etc. All these interactions may strongly affect the efficiency of drug delivery. Thus, studying the interaction of multilayer capsules with model cell cultures *in vitro* is a crucial step in their preliminary assessment as tools for targeted delivery. The use of both individual cell lines and more complex cell models (e.g., co-cultured cells and three-dimensional cell models (tumor spheroids) represents a comprehensive *in vitro* approach to modeling capsule–cancer cell interactions. Another problem that remains largely unstudied is *in vivo* delivery and tumor targeting of the capsules. The most interesting and promising approach in this area is the use of mouse models with xenografted human tumor cells. In these models, various characteristics of human cancer cells can be analyzed under the conditions close to those in the human body. Microparticles can interact with immune cells, such as macrophages and monocytes, be coated with nonspecific proteins and other molecules, and be nonspecifically captured by different cells. Selection of optimal strategies for administration of the capsules, as well as optimal dosing regimens, to ensure capsule targeted delivery and accumulation in the tumor growth area *in vivo* also represent one of the potential research lines in proof-of-the-concept studies of capsule-based delivery tools. However, the number of complete studies investigating the biodistribution and fate of Ab-functionalized multilayer capsules loaded with anticancer drugs is negligible. In this connection, studies on targeted drug-loaded multilayer capsules designed for the delivery to tumors are a promising trend that can help to analyze the efficiency of the designed capsule-based carriers.

Author Contributions

Conceptualization, A.S. and I.N.; data curation, G.N., T.T.; formal analysis, G.N, T.T., A.K.; funding acquisition, I.N.; project administration: A.S., supervision, I.N.; validation, A.K.; writing – original draft, G.N., A.S.; writing – review & editing, all authors.

Conflicts of interest

There are no conflicts to declare.

Acknowledgements

This work was supported by the French National Research Agency (ANR-20-CE19-009-02) and by the European Union with the European Regional Development Fund (FreeBioWave project) in its part related to the development of new surface chemistry approaches.

Notes and references

1 A. M. Pavlov, S. A. Gabriel, G. B. Sukhorukov and D. J. Gould, *Nanoscale*, 2015, **7**, 9686–9693.

2 C. E. Hansen, D. R. Myers, W. H. Baldwin, Y. Sakurai, S. L. Meeks, L. A. Lyon and W. A. Lam, *ACS Nano*, 2017, **11**, 5579–5589

3 J. J. Richardson, M. Y. Choy, J. Guo, K. Liang, K. Alt, Y. Ping, J. Cui, L. S. Law, C. E. Hagemeyer and F. Caruso, *Adv. Mater. (Weinheim, Ger.)*, 2016, **28**, 7703–7707.

4 J. Chen, S. Ratnayaka, A. Alford, V. Kozlovskaya, F. Liu, B. Xue, K. Hoyt and E. Kharlampieva, *ACS Nano*, 2017, **11**, 3135–3146.

5 A. Biswas, S. Banerjee, E. V. Gart, A. T. Nagaraja and M. J. McShane, *ACS Omega*, 2017, **2**, 2499–2506.

6 T. Paulraj, S. Wennmalm, A. V. Riazanova, Q. Wu, G. A. Crespo and A. J. Svagan, *ACS Appl. Mater. Interfaces*, 2018, **10**, 41146–41154.

7 Y.-H. You, A. Biswas, A. T. Nagaraja, J.-H. Hwang, G. L. Cote and M. J. McShane, *ACS Appl. Mater. Interfaces*, 2019, **11**, 14286–14295.

8 R. Bilan, A. Ametzazurra, K. Brazhnik, S. Escorza, D. Fernández, M. Uríbarri, I. Nabiev and A. Sukhanova, *Sci. Rep.*, 2017, **7**, 44668.

9 E. Marin, N. Tiwari, M. Calderón, J. R. Sarasua and A. Larrañaga, *ACS Appl. Mater. Interfaces*, 2021, **13**, 18511–18524.

10 G. Nifontova, M. Zvaigzne, M. Baryshnikova, E. Korostylev, F. Ramos-Gomes, F. Alves, I. Nabiev and A. Sukhanova, *Nanoscale Res. Lett.*, 2018, **13**, 30.

11 G. Nifontova, F. Ramos-Gomes, M. Baryshnikova, F. Alves, I. Nabiev and A. Sukhanova, *Front. Chem. (Lausanne, Switz.)*, 2019, **7**, 34.

12 N. Habibi, L. Pastorino, G. Babolmorad, C. Ruggiero, T. Guda and J. L. Ong, *J. Drug Delivery Sci. Technol.*, 2017, **38**, 1–8.

13 M. Björnmalm, A. Roozmand, K. F. Noi, J. Guo, J. Cui, J. J. Richardson and F. Caruso, *Langmuir*, 2015, **31**, 9054–9060.

14 L. Zhang, L.-H. Cai, P. S. Lienemann, T. Rossow, I. Polenz, Q. Vallmajo-Martin, M. Ehrbar, H. Na, D. J. Mooney and D. A. Weitz, *Angew. Chem., Int. Ed. Engl.*, 2016, **55**, 13470–13474.

15 G. Duan, M. F. Haase, K. J. Stebe and D. Lee, *Langmuir*, 2017, **34**, 847–853.

16 J. J. Richardson, D. Teng, M. Bjo, S. T. Gunawan, J. Guo, J. Cui, G. V. Franks and F. Caruso, *Langmuir*, 2014, **30**, 10028–10034.

17 K. F. Noi, A. Roozmand, M. Björnmalm, J. J. Richardson, G. V. Franks and F. Caruso, *ACS Appl. Mater. Interfaces*, 2015, **7**, 27940–27947.

18 Q. Wang and J. B. Schlenoff, *Adv. Mater. (Weinheim, Ger.)*, 2015, **27**, 2077–2082.

19 V. Calabrese, D. Califano, M. A. da Silva, J. Schmitt, S. J. Bryant, K. M. Z. Hossain, A. M. Percebom, A. Pérez Gramatges, J. L. Scott and K. J. Edler, *ACS Appl. Polym. Mater.*, 2020, **2**, 1213–1221.

20 M. Rasekh, Z. Ahmad, R. Barrie, M. Cross, J. H. Gil, J. D. E. T. Wilton-Ely and P. W. Miller, *Mol. Pharmaceutics*, 2017, **14**, 2010–2023.

21 D. B. Trushina, T. V. Bukreeva, T. N. Borodina, D. D. Belova, S. Belyakov and M. N. Antipina, *Colloids Surf., B*, 2018, **170**, 312–321.

22 A. S. Timin, A. R. Muslimov, A. V. Petrova, K. V. Lepik, M. V. Okilova, A. V. Vasin, B. V. Afanasyev and G. B. Sukhorukov, *Sci. Rep.*, 2017, **7**, 102.

23 C. Ganas, A. Weiß, M. Nazarenus, S. Rösler, T. Kissel, P. Rivera Gil and W. J. Parak, *J. Controlled Release*, 2014, **196**, 132–138.

24 V. V. Serra, R. Teixeira, S. M. Andrade and S. M. B. Costa, *Colloids Surf., B*, 2016, **146**, 127–135.

25 H. Gao, O. A. Goriacheva, N. V. Tarakina and G. B. Sukhorukov, *ACS Appl. Mater. Interfaces*, 2016, **8**, 9651–9661.

26 Y. Yang, H. Zhu, J. Wang, Q. Fang and Z. Peng, *ACS Appl. Mater. Interfaces*, 2018, **10**, 33493–33506.

27 D. Piccinino, E. Capecchi, L. Botta, B. M. Bizzari, P. Bollella, R. Antiochia and R. Saladino, *Biomacromolecules*, 2018, **19**, 3883–3893.

28 S. Beyer, R. Schürmann, I. Feldmann, A. Blocki, I. Bald, R. J. Schneider and F. Emmerling, *Colloid Interface Sci. Commun.*, 2018, **22**, 14–17.

29 D. Zhou, H. Xiao, F. Meng, S. Zhou, J. Guo, X. Li, X. Jing and Y. Huang, *Bioconjugate Chem.*, 2012, **23**, 2335–2343.

30 X. Guo, K. S. Golzales and D. M. Lynn, *Chem. Mater.*, 2019, **31**, 7443–7452.

31 A. Alford, M. Rich, V. Kozlovskaya, J. Chen, J. Sherwood, M. Bolding, J. Warram, Y. Bao and E. Kharlampieva, *Adv. Ther. (Weinheim, Ger.)*, 2018, **1**, 1800051.

32 L. Chen, H. An and P. S. Doyle, *Langmuir*, 2015, **31**, 9228–9235.

33 A. R. Ibragimova, A. B. Mirgorodskaya, E. A. Vasilieva, E. I. Khairutdinova, T. K. Meleshko, I. V. Ivanov, A. V. Yakimansky, I. R. Nizameev, M. K. Kadirov and L. Y. Zakharova, *Colloids Surf., A*, 2016, **526**, 20–28.

34 Y. Zhang, G. Zhu, B. Dong, J. Tang, J. Li, G. Yang, S. Hong and F. Xing, *ACS Appl. Mater. Interfaces*, 2019, **11**, 43741–43750.

35 Q. Ma, Y. Song, J. W. Kim, H. S. Choi and H. C. Shum, *ACS Macro Lett.*, 2016, **5**, 666–670.

36 G. Kaufman, S. Nejati, R. Sarfati, R. Boltyanskiy, M. Loewenberg, E. R. Dufresne and C. O. Osuji, *Soft Matter*, 2015, **11**, 7478–7482.

37 O. A. Inozemtseva, D. V. Voronin, A. V. Petrov, V. V. Petrov, S. A. Lapin, A. A. Kozlova, D. N. Bratashov, A. M. Zakharevich and D. A. Gorin, *Colloid J.*, 2019, **80**, 771–782.

38 H. Shen, F. Li, D. Wang, Z. Yang, C. Yao, Y. Ye and X. Wang, *Drug Des., Dev. Ther.*, 2018, **12**, 921–934.

39 A. Alford, B. Tucker, V. Kozlovskaya, J. Chen, N. Gupta, R. Caviedes, J. Gearhart, D. Graves and E. Kharlampieva, *Polymers*, 2018, **10**, 1342.

40 V. Kozlovskaya, J. Chen, O. Zavgorodnya, M. B. Hasan and E. Kharlampieva, *Langmuir*, 2018, **34**, 11832–11842.

41 Y. Tarakanchikova, J. Alzubi, V. Pennucci, M. Follo, B. Kochergin, A. Muslimov, I. Skovorodkin, S. Vainio, M. N. Antipina, V. Atkin, A. Popov, I. Meglinski, T. Cathomen, T. I. Cornu, D. A. Gorin, G. B. Sukhorukov and I. Nazarenko, *Small*, 2019, **16**, 1904880.

42 S. Roy, N. M. Elbaz, W. J. Parak and N. Feliu, *ACS Applied Bio Materials*, 2019, **2**, 3245–3256.

43 A. K. Locke, A. K. Means, P. Dong, T. Nichols, G. L. Cote and M. A. Grunlan, *ACS Appl. Bio Mater.*, 2018, **1**, 1319–1327.

44 A. L. Popov, N. Popova, D. J. Gould, A. B. Shcherbakov, G. B. Sukhorukov and V. K. Ivanov, *ACS Appl. Mater. Interfaces*, 2018, **10**, 14367–14377.

45 T. A. Kolesnikova, G. Kiragosyan, T. H. N. Le, S. Springer and M. Winterhalter, *ACS Applied Materials and Interfaces*, 2017, **9**, 11506–11517.

46 M. V. Novoselova, H. M. Loh, D. B. Trushina, A. Ketkar, T. O. Abakumova, T. S. Zatsepin, M. Kakran, A. M. Brzozowska, H. H. Lau, D. A. Gorin, M. N. Antipina and A. I. Brichkina, *ACS Appl. Mater. Interfaces*, 2020, **12**, 5610–5623.

47 A. S. Timin, K. V. Lepik, A. R. Muslimov, D. A. Gorin, B. V. Afanasyev and G. B. Sukhorukov, *Colloids Surf., B*, 2016, **147**, 450–458.

48 V. Milosavljevic, E. Jamróz, M. Gagic, Y. Haddad, H. Michalkova, R. Balkova, B. Tesarova, A. Moulick, Z. Heger, L. Richtera, P. Kopel and V. Adam, *Biomacromolecules*, 2020, **21**, 418–434.

49 X. Sun, C. Liu, A. M. Omer, L.-Y. Yang and X. Ouyang, *Int. J. Biol. Macromol.*, 2019, **132**, 487–494.

50 R. Akasov, T. Borodina, E. Zaytseva, A. Sumina, T. Bukreeva, S. Burov and E. Markvicheva, *ACS Appl. Mater. Interfaces*, 2015, **7**, 16581–16589.

51 L. van der Meeren, J. Li, M. Konrad, A. G. Skirtach, D. Volodkin and B. V. Parakhonskiy, *Macromol. Biosci.*, 2020, **20**, 2000081.

52 A. L. Becker, N. I. Orlotti, M. Folini, F. Cavalieri, A. N. Zelikin, A. P. R. Johnston, N. Zaffaroni and F. Caruso, *ACS Nano*, 2011, **5**, 1335–1344.

53 S. Rahimian, M. F. Fransen, J. W. Kleinovink, M. Amidi, F. Ossendorp and W. E. Hennink, *Biomaterials*, 2015, **61**, 33–40.

54 S. Pulakkat, S. A. Balaji, A. Rangarajan and A. M. Raichur, *ACS Appl. Mater. Interfaces*, 2016, **8**, 23437–23449.

55 J. Cui, K. Alt, Y. Ju, S. T. Gunawan, J. A. Braunger, T.-Y. Wang, Y. Dai, Q. Dai, J. J. Richardson, J. Guo, M. Björnmalm, C. E. Hagemeyer and F. Caruso, *Biomacromolecules*, 2019, **20**, 3592–3600.

56 B. Xue, V. Kozlovskaya, M. A. Sherwani, S. Ratnayaka, S. Habib, T. Anderson, M. Manuvakhova, L. Klampfer, N. Yusuf and E. Kharlampieva, *Biomacromolecules*, 2018, **19**, 4084–4097.

57 K. G. Reuter, J. L. Perry, D. Kim, J. C. Luft, R. Liu and J. M. DeSimone, *Nano Lett.*, 2015, **15**, 6371–6378.

58 A. M. Hafner, D. Burschowsky, B. Corthésy, M. Textor and H. P. Merkle, *J. Controlled Release*, 2012, **159**, 204–214.

59 Q. Dai, Y. Yan, C.-S. Ang, K. Kempe, M. M. J. Kamphuis, S. J. Dodds and F. Caruso, *ACS Nano*, 2015, **9**, 2876–2885.

60 D. M. Richards and R. G. Endres, *Biophys. J.*, 2014, **107**, 1542–1553.

61 B. A. Holt, M. C. Bellavia, D. Potter, D. White, S. R. Stowell and T. Sulchek, *Biomater. Sci.*, 2017, **5**, 463–474.

62 D. F. Canova, A. M. Pavlov, L. V. Norling, T. Gobbetti, S. Brunelleschi, P. le Fauder, N. Cenac, G. B. Sukhorukov and M. Perretti, *J. Controlled Release*, 2015, **217**, 284–292.

63 Q. Du, C. Fu, J. Tie, T. Liu, L. Li, X. Ren, Z. Huang, H. Liu, F. Tang, L. Li and X. Meng, *Nanoscale*, 2015, **7**, 3147–3154.

64 V. Kozlovskaya, M. Dolmat and E. Kharlampieva, *ACS Appl. Polym. Mater.* 2021, **3**, 2274–2289.

65 E. Marin, C. Tapeinos, J. R. Sarasua and A. Larrañaga, *Adv. Colloid Interface Sci.*, 2022, 304, 102680.

66 M. V. Zyuzin, A. S. Timin and G. B. Sukhorukov, *Langmuir*, 2019, **35**, 4747–4762.

67 Q. Dai, N. Bertleff-Zieschang, J. A. Braunger, M. Björnmalm, C. Cortez-Jugo and F. Caruso, *Adv. Healthc. Mater.*, 2018, **7**, 1700575.

68 J. Chen, V. Kozlovskaya, A. Goins, J. Campos-Gomez, M. Saeed and E. Kharlampieva, *Biomacromolecules*, 2013, **14**, 3830–3841.

69 P. Shi, J. Qin, X. Wu, L. Wang, T. Zhang, D. Yang, X. Zan and D. Appelhans, *ACS Appl. Mater. Interfaces*, 2019, **11**, 39209–39218.

70 A. V. Ermakov, R. A. Verkhovskii, I. V. Babushkina, D. B. Trushina, O. A. Inozemtseva, E. A. Lukyanets, V. J. Ulyanov, D. A. Gorin, S. Belyakov and M. N. Antipina, *Pharmaceutics*, 2020, **12**, 610.

71 X. Liu, D. Appelhans, Q. Wei and B. Voit, *Adv. Sci.*, 2016, **4**, 1600308.

72 M. Li, R. L. Harbron, J. V. M. Weaver, B. P. Binks and S. Mann, *Nat. Chem.*, 2013, **5**, 529–536.

73 N. Hu, J. Frueh, C. Zheng, B. Zhang and Q. He, *Colloids Surf., A*, 2015, **17**, 315-323.

74 F. Liu, V. Kozlovskaya, O. Zavgorodnya, C. Martinez-Lopez, S. Catledge and E. Kharlampieva, *Soft Matter*, 2014, **10**, 9237–9247.

75 K. Liang, G. K. Such, A. P. R. Johnston, Z. Zhu, H. Ejima, J. J. Richardson, J. Cui and F. Caruso, *Adv. Mater. (Weinheim, Ger.)*, 2014, **26**, 1901–1905.

76 J. M. Silva, S. G. Caridade, R. R. Costa, N. M. Alves, T. Groth, C. Picart, R. L. Reis and J. F. Mano, *Langmuir*, 2015, **31**, 11318–11328.

77 R. Hartmann, M. Weidenbach, M. Neubauer, A. Fery and W. J. Parak, *Angew. Chem., Int. Ed. Engl.*, 2015, **54**, 1365–1368.

78 S. Donatan, A. Yashchenok, N. Khan, B. Parakhonskiy, M. Cocquyt, B.-E. Pinchsik, D. Khalenkow, H. Möhwald, M. Konrad and A. Skirtach, *ACS Appl. Mater. Interfaces*, 2016, **8**, 14284–14292.

79 B. Parakhonskiy, M. V. Zyuzin, A. Yashchenok, S. Carregal-Romero, J. Rejman, H. Möhwald, W. J. Parak and A. G. Skirtach, *J. Nanobiotechnol.*, 2015, **13**, 53.

80 H. Bahrom, A. A. Goncharenko, L. Fatkhutdinova, O. Peltek, A. Muslimov, O. Koval, I. E. Eliseev, A. Manchev, D. Gorin, I.

Shishkin, R. E. Noskov, A. S. Timin, P. Ginzburg and M. V. Zyuzin, *ACS Sustainable Chem. Eng.*, 2019, **7**, 191412–19156.
81 E. Kilic, M. V. Novoselova, S. H. Lim, N. A. Pyataev, S. I. Pinyaev, O. A. Kulikov, O. A. Sindeeva, O. A. Mayorova, R. Murney, M. N. Antipina, B. Haigh, G. B. Sukhorukov and M. V. Kiryukhin, *Sci. Rep.*, 2017, **7**, 44159.
82 D. Song, J. Cui, Y. Ju, M. Faria, H. Sun, C. B. Howard, K. J. Thurecht and F. Caruso, *ACS Appl. Mater. Interfaces*, 2019, **11**, 28720–28731.
83 V. F. Korolovych, O. A. Grishina, O. A. Inozemtseva, A. V. Selifonov, D. N. Bratashov, S. G. Suchkov, L. A. Bulavin, O. E. Glukhova, G. B. Sukhorukov and D. A. Gorin, *Phys. Chem. Chem. Phys.*, 2015, **18**, 2389–2397.
84 I. E. Palama, S. Leporatti, E. de Luca, N. di Renzo, M. Maffia, C. Gambacorti-Passerini, R. Rinaldi, G. Gigli, R. Cingolani and A. M. L. Coluccia, *Nanomedicine (London, U.K.)*, 2010, **5**, 419–431.
85 V. Vergaro, P. Papadia, P. Petrini, F. P. Fanizzi, S. A. de Pascali, F. Baldassarre, L. Pastorino and G. Ciccarella, *Int. J. Biol. Macromol.*, 2017, **99**, 187–195.
86 M. V. Zyuzin, P. Díez, M. Goldsmith, S. Carregal-Romero, C. Teodosio, J. Rejman, N. Feliu, A. Escudero, M. J. Almendral, U. Linne, D. Peer, M. Fuentes and W. J. J. Parak, *Bioconjugate Chem.*, 2017, **28**, 556–564.
87 A. Garapaty and J. A. Champion, *Bioeng. Transl. Med.*, 2017, **2**, 92–101.
88 C. Cortez, E. Tomaskovic-Crook, A. P. R. Johnston, A. M. Scott, E. C. Nice, J. K. Heath and F. Caruso, *ACS Nano*, 2007, **1**, 93–102.
89 V. Kozlovskaya, J. F. Alexander, Y. Wang, T. Kuncewicz, X. Liu, B. Godin and E. Kharlampieva, *ACS Nano*, 2014, **8**, 5725–5737.
90 X. Chen, Y. Yan, M. Müllner, Y. Ping, J. Cui, K. Kempe, C. Cortez-Jugo and F. Caruso, *Biomacromolecules*, 2016, **17**, 1205–1212.
91 J. Zhu, C. Sevencan, M. Zhang, R. S. A. McCoy, X. Ding, J. Ye, J. Xie, K. Ariga, J. Feng, B. H. Bay and D. T. Leong, *ACS Nano*, 2020, **14**, 3259–3271.
92 M. Björnmalm, M. Faria, X. Chen, J. Cui and F. Caruso, *Langmuir*, 2016, **32**, 10995–11001.
93 D. Ma, S. Tian, J. Baryza, J. C. Luft and J. M. DeSimone, *Mol. Pharmaceutics*, 2015, **12**, 3518–3526.
94 X. Liu, H. Zheng, G. Li, H. Li, P. Zhang, W. Tong and C. Gao, *Colloids Surf., B*, 2017, **158**, 675–681.
95 H. Li, W. Zhang, W. Tong and C. Gao, *ACS Appl. Mater. Interfaces*, 2016, **8**, 11210–11214.
96 M. Brueckner, S. Jankuhn, E. M. Jülke and U. Reibetanz, *Int. J. Nanomed.*, 2018, **13**, 2079–2091.
97 S. Rutkowski, T. Si, M. Gai, M. Sun, J. Frueh and Q. He, *J. Colloid Interface Sci.*, 2019, **541**, 407–417.
98 H. Sun, E. H. H. Wong, Y. Yan, J. Cui, Q. Dai, J. Guo, G. G. Qiao and F. Caruso, *Chem. Sci.*, 2015, **6**, 3505–3514.
99 A. Salis, M. Fanti, L. Medda, V. Nairi, F. Cugia, M. Piludu, V. Sogos and M. Monduzzi, *ACS Biomater. Sci. Eng.*, 2016, **2**, 741–751.
100 D. V. Voronin, O. A. Sindeeva, M. A. Kurochkin, O. Mayorova, I. V. Fedosov, O. Semyachkina-Glushkovskaya, D. A. Gorin, V. V. Tuchin and G. B. Sukhorukov, *ACS Appl. Mater. Interfaces*, 2017, **9**, 6885–6893.
101 G. Nifontova, A. Efimov, O. Agapova, I. Agapov, I. Nabiev and A. Sukhanova, *Nanoscale Res. Lett.*, 2019, **14**, 29.
102 Q. Dai, J. Guo, Y. Yan, C. S. Ang, N. Bertleff-Zieschang and F. Caruso, *Biomacromolecules*, 2017, **18**, 431–439.103S. Łukasiewicz and K. Szczepanowicz, *Langmuir*, 2014, **30**, 1100–1107.
104 G. Baier, D. Baumann, J. M. Siebert, A. Musyanovych, V. Mailänder and K. Landfester, *Biomacromolecules*, 2012, **13**, 2704–2715.
105 H. Sun, J. Cui, Y. Ju, X. Chen, E. H. H. Wong, J. Tran, G. G. Qiao and F. Caruso, *Bioconjugate Chem.*, 2017, **28**, 1859–1866.
106 K. Szczepanowicz, T. Kruk, W. Swiatek, A. M. Bouzga, C. R. Simon and P. Warszynski, *Colloids Surf., B*, 2018, **166**, 295–302.
107 L. J. Chan, D. B. Ascher, R. Yadav, J. B. Bulitta, C. W. Charlotte, C. J. H. Porter, C. B. Landersdorfer and L. M. Kaminskas, *Mol. Pharmaceutics*, 2016, **13**, 1229–1241.
108 T. Liu, P. Song, A. Märcher, J. Kjems, C. Yang and K. V. Gothelf, *ChemBioChem*, 2019, **20**, 1014–1018.
109 V. Filipe, B. Kukrer, A. Hawe and W. Jiskoot, *J. Pharm. Sci.*, 2012, **101**, 2327–2339.
110 G. Rousserie, R. Grinevich, K. Brazhnik, K. Even-Desrumeaux, B. Reveil, T. Tabary, P. Chames, D. Baty, J. H. M. Cohen, I. Nabiev and A. Sukhanova, *Anal. Biochem.*, 2015, **478**, 26–32.
111 A. P. R. Johnston, M. M. J. Kamphuis, G. K. Such, A. M. Scott, E. C. Nice, J. K. Heath and F. Caruso, *ACS Nano*, 2012, **6**, 6667–6674.
112 G. Nifontova, D. Kalenichenko, M. Baryshnikova, F. R. Gomes, F. Alves, A. Karaulov, I. Nabiev and A. Sukhanova, *Photonics*, 2019, **6**, 117.
113 I. Pereira, F. Sousa, P. Kennedy and B. Sarmento, *Int. J. Pharm. (Amsterdam, Neth.)*, 2018, **549**, 397–403.
114 T. Patiño, J. Soriano, L. Barrios, E. Ibáñez and C. Nogués, *Sci. Rep.*, 2015, **5**, 11371.
115 M. Göse, K. Scheffler and U. Reibetanz, *Biomacromolecules*, 2016, **17**, 3672–3682.
116 C. J. Moore, H. Monton, R. O`Kennedy, D. E. Williams, C. Nogues, C. Crean (nee Lynam) and V. Gubala, *J. Mater. Chem. B*, 2015, **3**, 2043–2055.
117 K. Brazhnik, Z. Sokolova, M. Baryshnikova, R. Bilan, A. Efimov, I. Nabiev and A. Sukhanova, *Nanomedicine (N. Y., NY, U. S.)*, 2015, **11**, 1065–1075.
118 K. Totaro, X. Liao, K. Bhattacharya, J. I. Finneman, B. Justin, M. A. Massa, J. Thorn, S. V. Ho and B. L. Pentelute, *Bioconjugate Chem.*, 2016, **27**, 994–1004.
119 T. G. Shutava, K. S. Livanovich and V. V. Pankov, *Colloids Surf., A*, 2017, **539**, 69–79.
120 M. V. Zyuzin, Y. Yan, R. Hartmann, K. T. Gause, M. Nazarenus, J. Cui, F. Caruso and W. J. Parak, *Bioconjugate Chem.*, 2017, **28**, 2062–2068.

121 M. V. Zyuzin, D. Antuganov, Y. V. Tarakanchikova, T. E. Karpov, T. V. Mashel, E. N. Gerasimova, O. O. Peltek, N. Alexandre, S. Bruyere, Y. A. Kondratenko, A. R. Muslimov and A. S. Timin, *ACS Appl. Mater. Interfaces*, 2020, **12**, 31137–31147.

122 S. Winzen, S. Schoettler, G. Baier, C. Rosenauer, V. Mailaender, K. Landfester and K. Mohr, *Nanoscale*, 2015, **7**, 2992–3001.

123 K. Yong, D. Yuen, M. Z. Chen and A. P. R. Johnston, *ACS Appl. Mater. Interfaces*, 2020, **12**, 5593–5600.

124 D. I. Deo, J. E. Gautrot, G. B. Sukhorukov and W. Wang, *Biomacromolecules*, 2014, **15**, 2555–2562.

125 S. K. Verma, A. Amoah, U. Schellhaas, M. Winterhalter, S. Springer and T. A. Kolesnikova, *Adv. Funct. Mater.*, 2016, **26**, 6015–6024.

126 J. Cui, Y. Ju, Z. H. Houston, J. J. Glass, N. L. Fletcher, S. Alcantara, Q. Dai, C. B. Howard, S. M. Mahler, A. K. Wheatley, R. de Rose, P. T. Brannon, B. M. Paterson, P. S. Donnelly, K. J. Thurecht, F. Caruso and S. J. Kent, *Adv. Healthcare Mater.*, 2019, **8**, 1801607.

127 J. S. Lewis, T. D. Zaveri, C. P. Crooks and B. G. Keselowsky, *Biomaterials*, 2012, **33**, 7221–7232.

128 C. Zhan, B. Gu, C. Xie, J. Li, Y. Liu and W. Lu, *J. Controlled Release*, 2010, **143**, 136–142.

129 A. Taschauer, W. Polzer, F. Alioglu, M. Billerhart, S. Decker, T. Kittelmann, E. Geppl, S. Elmenofi, M. Zehl, E. Urban, H. Sami and M. Ogris, *Mol. Ther.--Nucleic Acids*, 2019, **18**, 774–786.

130 K. Zarschler, K. Prapainop, E. Mahon, L. Rocks, M. Bramini, P. M. Kelly, H. Stephan and K. A. Dawson, *Nanoscale*, 2014, **6**, 6046–6056.

131 D. G. Belair, M. J. Miller, S. Wang, S. R. Darjatmokon, B. Y. K. Binder, N. Sheibani and W. L. Murphy, *Biomaterials*, 2016, **93**, 27–37.

132 J. S. Buhrman, L. C. Cook, J. E. Rayahin, M. J. Federle and R. A. Gemeinhart, *J. Controlled Release*, 2013, **171**, 288–295.

133 B. A. Evans, J. C. Ronecker, D. T. Han, D. R. Glass, T. L. Train and A. E. Deatsch, *Mater. Sci. Eng., C*, 2016, **62**, 860–869.

134 W. Liu, X. Wang, K. Bai, M. Lin, G. Sukhorukov and W. Wang, *J. R. Soc., Interface*, 2014, **11**, 20141027.

135 P. Scodeller, P. N. Catalano, N. Salguero, H. Duran, A. Wolosiuk and G. J. A. A. Soler-Illia, *Nanoscale*, 2013, **5**, 9690–9698.

136 Y. Ju, Q. Dai, J. Cui, Y. Dai, T. Suma, J. J. Richardson and F. Caruso, *ACS Appl. Mater. Interfaces*, 2016, **8**, 22914–22922.

137 M. P. Melancon, M. Zhou, R. Zhang, C. Xiong, P. Allen, X. Wen, Q. Huang, M. Wallace, J. N. Myers, R. J. Stafford, D. Liang, A. D. Ellington and C. Li, *ACS Nano*, 2014, **8**, 4530–4538.

138 A. C. G. Weiss, K. Krüger, Q. A. Besford, M. Schlenk, K. Kempe, S. Förster and F. Caruso, *ACS Appl. Mater. Interfaces*, 2019, **11**, 2459–2469.

139 P. Pacheco, D. White and T. Sulchek, *PLoS ONE*, 2013, **8**, e60989.

140 Q. Dai, Y. Yan, J. Guo, M. Björnmalm, J. Cui, H. Sun and F. Caruso, *ACS Macro Lett.*, 2015, **4**, 1259–1263.

141 G. Yun, J. J. Richardson, M. Capelli, Y. Hu, Q. A. Besford, A. C. G. Weiss, H. Lee, I. S. Choi, B. C. Gibson, P. Reineck and F. Caruso, *Adv. Funct. Mater.*, 2019, **30**, 1905805.

142 C. Sóñora, P. Arbildi, I. Miraballes-Martínez and A. Hernández, *J. Immunoassay Immunochem.*, 2018, **39**, 70–83.

143 A. C. G. Weiss, H. G. Kelly, M. Faria, Q. A. Besford, A. K. Wheatley, C.-S. Ang, E. J. Crampin, F. Caruso and S. J. Kent, *ACS Nano*, 2019, **13**, 4980–4991.

144 M. Djaldetti and H. Bessler, *Biomed. Pharmacother.*, 2014, **68**, 679–683.

145 A. Romoser, D. Ritter, R. Majitha, K. E. Meissner, M. McShane and C. M. Sayes, *PLoS ONE*, 2011, **6**, e22079.

146 J. Song, Y. Ju, T. H. Amarasena, Z. Lin, S. Mettu, J. Zhou, M. A. Rahim, C. S. Ang, C. Cortez-Jugo, S. J. Kent and F. Caruso, *ACS Nano*, 2021, **15**, 10025–10038.

147 K. Vahidkhah and P. Bagchi, *Soft Matter*, 2015, **11**, 2097–2109.

148 D. Song, J. Cui, H. Sun, T. H. Nguyen, S. Alcantara, R. de Rose, S. J. Kent, C. J. H. Porter and F. Caruso, *ACS Appl. Mater. Interfaces*, 2017, **9**, 33683–33694.

149 L. Kastl, D. Sasse, V. Wulf, R. Hartmann, J. Mircheski, C. Ranke, S. Carregal-Romero, J. A. Martínez-López, R. Fernández-Chacón, W. J. Parak, H.-P. Elsasser and P. Rivera Gil, *ACS Nano*, 2013, **7**, 6605–6618.

150 Y. Yan, A. P. R. Johnston, S. J. Dodds, M. M. J. Kamphuis, C. Ferguson, R. G. Parton, E. C. Nice, J. K. Heath and F. Caruso, *ACS Nano*, 2010, **4**, 2928–2936.

151 A. Osswald, V. Hedrich and W. Sommergruber, in *Target Identification and Validation in Drug Discovery: Methods and Protocols,* eds. J. Moll and S. Carotta, Humana Press, New York, NY, 2019, vol. 1953, pp. 151–162.

152 S. P. Rebelo, C. Pinto, T. R. Martins, N. Harrer, M. F. Estrada, P. Loza-Alvarez, J. Cabeçadas, P. M. Alves, E. J. Gualda, W. Sommergruber and C. Brito, *Biomaterials*, 2018, **163**, 185–197.

153 E. Shahar, R. Gorodetsky, E. Gaberman, E. Aizenshtein and J. Pitcovski, *Vaccine*, 2010, **28**, 7279–7287.

154 A. S. Timin, A. R. Muslimov, K. V. Lepik, M. V. Okilova, N. Y. Tcvetkov, A. I. Shakirova, B. V. Afanasyev, D. A. Gorin and G. B. Sukhorukov, *Part. Part. Syst. Charact.*, 2017, **34**, 1600417.

155 A. R. Muslimov, A. S. Timin, V. R. Bichaykina, O. O. Peltek, T. E. Karpov, A. Dubavik, A. Nominé, J. Ghanbaja, G. B. Sukhorukov and M. V. Zyuzin, *Biomaterials Sci.*, 2020, **8**, 1137–1147.

156 A. S. Timin, O. O. Peltek, M. V. Zyuzin, A. R. Muslimov, T. E. Karpov, O. S. Epifanovskaya, A. I. Shakirova, M. V. Zhukov, Y. V. Tarakanchikova, K. V. Lepik, V. S. Sergeev, G. B. Sukhorukov and B. V. Afanasyev, *ACS Appl. Mater. Interfaces*, 2019, **11**, 13091–13104.

157 Q. Sun, Y. Du, E. A. H. Hall, D. Luo, G. B. Sukhorukov and A. F. Routh, *Soft Matter*, 2018, **14**, 2594–2603.

158 M. H. Bakalar, A. M. Joffe, E. M. Schmid, S. Son, M. Podolski, D. A. Fletcher, M. H. Bakalar, A. M. Joffe, E. M. Schmid, S. Son, M. Podolski and D. A. Fletcher, *Cell*, 2018, **174**, 131–142.

159 Z. Lin, W. Gao, H. Hu, K. Ma, B. He, W. Dai, X. Wang, J. Wang, X. Zhang and Q. Zhang, *J. Controlled Release*, 2014, **174**, 161–170.

160 K. B. Ghaghada, Z. A. Starosolski, A. Lakoma, C. Kaffes, S. Agarwal, K. K. Athreya, J. Shohet, E. Kim and A. Annapragada, *PLoS ONE*, 2016, **11**, e0165877.

161 A. Jain, R. Jain, S. Jain, R. Khatik and D. Veer Kohli, *Artif. Cells, Nanomed., Biotechnol.*, 2019, **47**, 1085–1093.

162 J. F. Alexander, V. Kozlovskaya, J. Chen, T. Kuncewicz, E. Kharlampieva and B. Godin, *Adv. Healthcare Mater.*, 2015, **4**, 2657–2666.

163 N. Mustafaoglu, N. J. Alves and B. Bilgicer, *Langmuir*, 2015, **31**, 9728–9736.

164 M. Röhm, A. Handl and M. König, *Data Brief*, 2016, **8**, 426–435.

165 J. Liu, X. Shan, X. Su, Z. Hu and B. Wang, *Colloids Surf., A*, 2020, **605**, 125354.

List of Figures

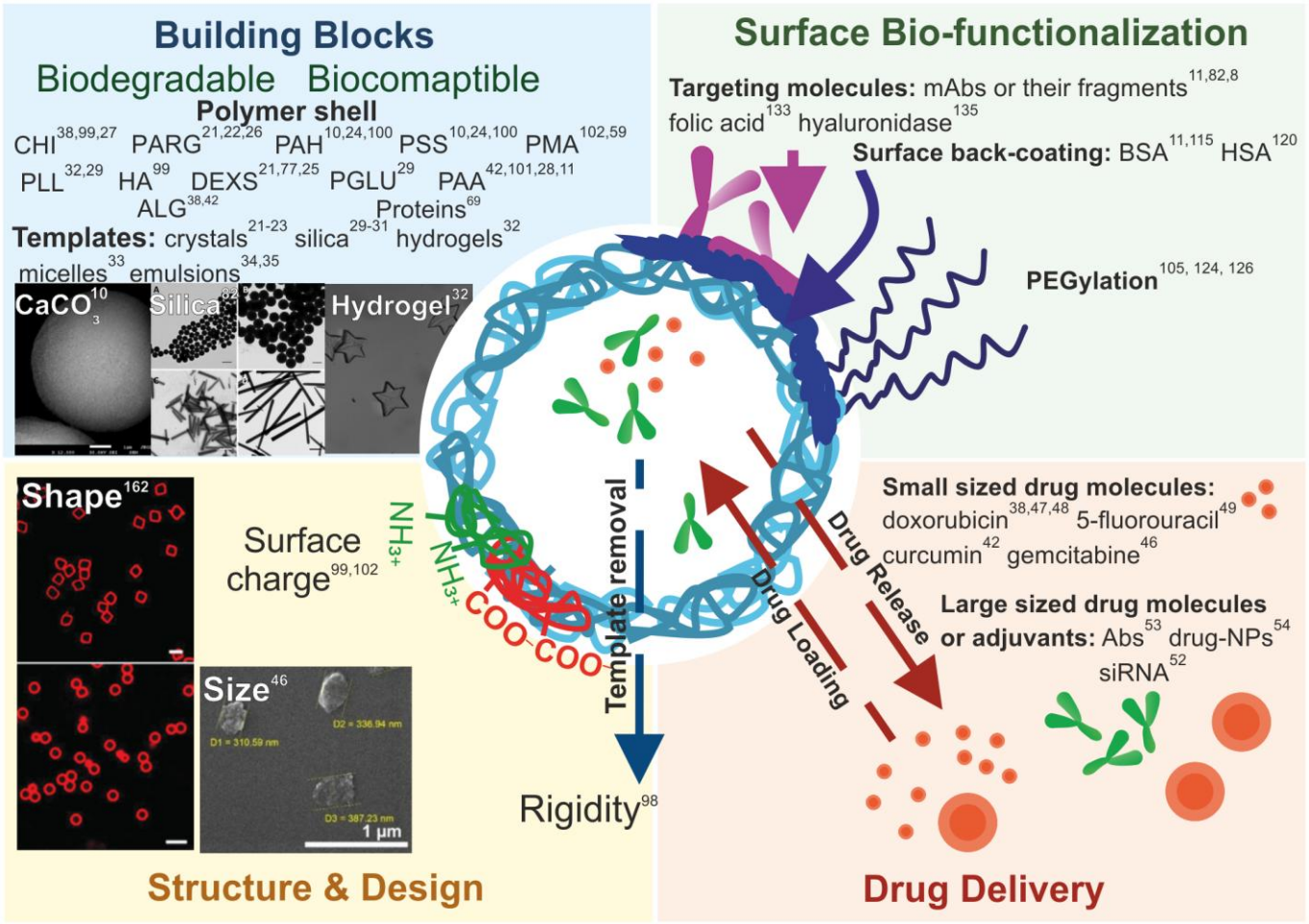

Fig. 1. Design of a capsule-based delivery system targeted to molecular markers.
The effectiveness of cancer cell targeting of the capsule-based delivery tools is determined by the structural components used in their engineering and the size, shape, and surface characteristics, including additional modification with targeting molecules (vectors) enabling highly specific capsule–cell interaction and capsule affinity to target cells, surface back-coating to enhance capsule biocompatibility, and additional PEGylation to reduce opsonization and interaction with the immune system cells.
Abbreviations: PARG, polyarginin; PAH, polyallyamine hydrochloride; PSS, poly(sodium styrene sulfonate); PMA, polymethacrylic acid; PLL, poly-L-lysine; HA, hyaluronic acid; DEXS, dextran sulfate; PGLU, polyglutamic acid; PAA, polyacrylic acid and its derivatives; ALG, alginic acid; BSA, bovine serum albumin; HSA, human serum albumin; PEG, polyethylene glycol; Abs, antibodies; NPs, nanoparticles, siRNA, small interfering ribonucleic acid.
The microphotographs of calcium carbonate microparticles are adapted from Nifontova *et al.*[10], and silica particles and hydrogels, from Song *et al.*[82] and Chen *et al.*[32], respectively. The shape and size characteristics of the capsules are adapted from Alexander *et al.*[162] and Novoselova *et al.*[46], respectively.

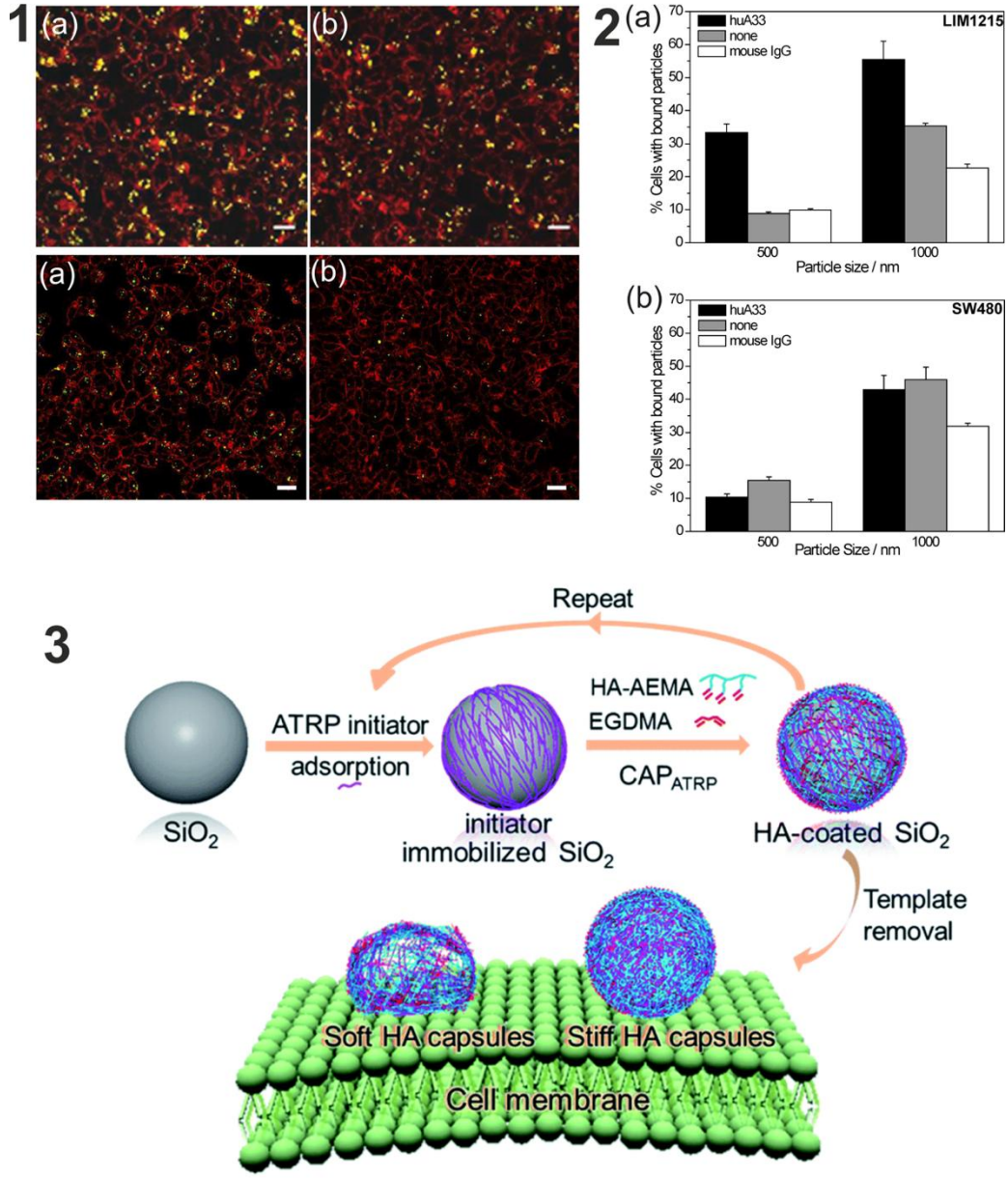

Fig. 2. The effects of particle size and rigidity on capsule–cell interaction.

Panel 1: The effect of capsule size on particle–cell interaction and efficiency of cancer cell targeting. Representative merged confocal laser scanning microscopy images of fluorescein-labeled (a) huA33 monoclonal antibody (mAb)-coated, (b) noncoated 1-μm capsules (upper raw) and (a) huA33 mAb-coated, (b) noncoated ~500-nm capsules (lower raw). The capsules (shown in yellow) were incubated with living cells for 6 h to allow particle–cell interaction. Cell membranes were counter-stained with the mouse mAb against the epidermal growth factor receptor (EGFR) (mAb 528) and detected with tetramethylrhodamine (TRITC)-conjugated anti-mouse secondary immunoglobulin G (IgG) antibody (red). Scale bars, 10 μm. Adapted from Cortez *et al.* [88] and from Suppl. Materials of Cortez *et al.* [88].

Panel 2: The effect of particle size on the selective binding of particles to cells. Binding of fluorescently labeled huA33 mAb-coated, noncoated, and mouse IgG-coated core/shell particles (500 nm and 1 μm) to (a) A33 antigen-expressing LIM1215 cells and (b) SW480 cells not expressing the A33 antigen. The ordinate axis shows the percentage of live cells with bound particles after 1 h of incubation at 4°C, as analyzed by flow cytometry. Adapted from Cortez *et al.*[88].

Panel 3: Scheme of soft/rigid capsule fabrication and illustration of their differences in the characteristics of attachment to the cell membrane and their cell surface binding behaviour (capsules were prepared by means of continuous assembly of polymers (CAP$_{ATRP}$) using silicon dioxide particles as templates, which includes ATRP (macroinitiator P(METAOTs-*co*-BIEM) adsorption, ATRP-promoted hyaluronic acid (HA) film growth, and template removal). Adapted from Sun *et al.*[98].

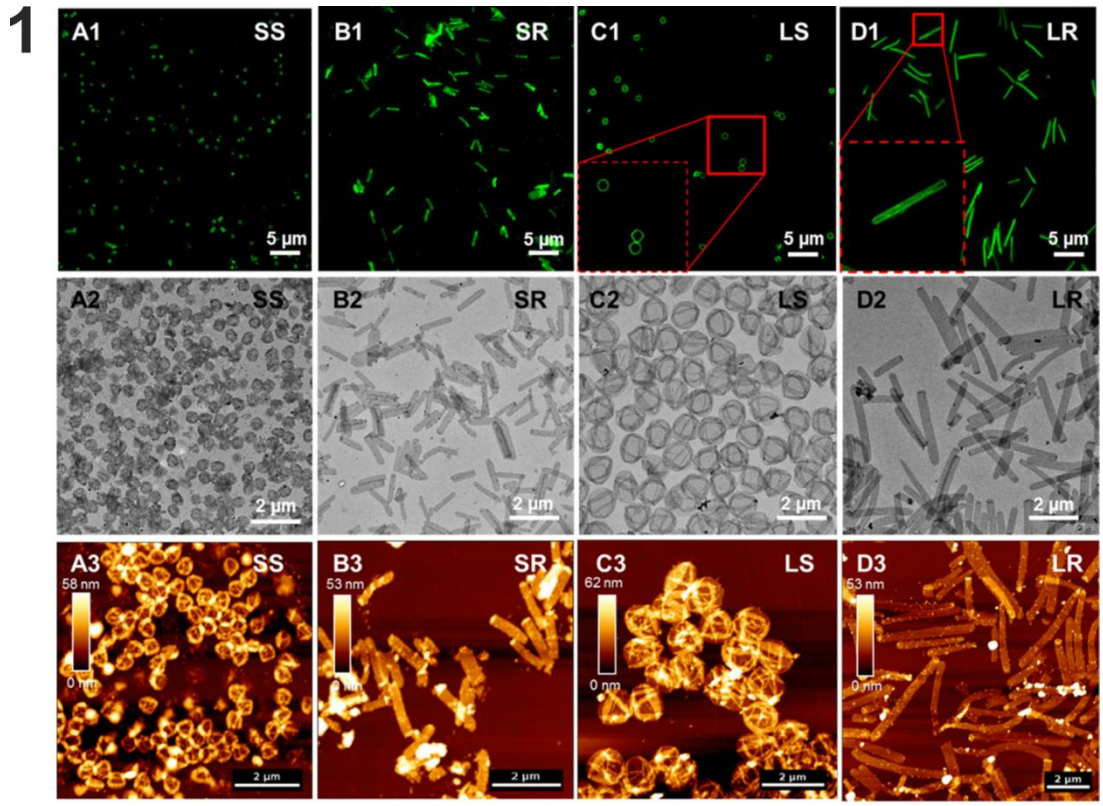

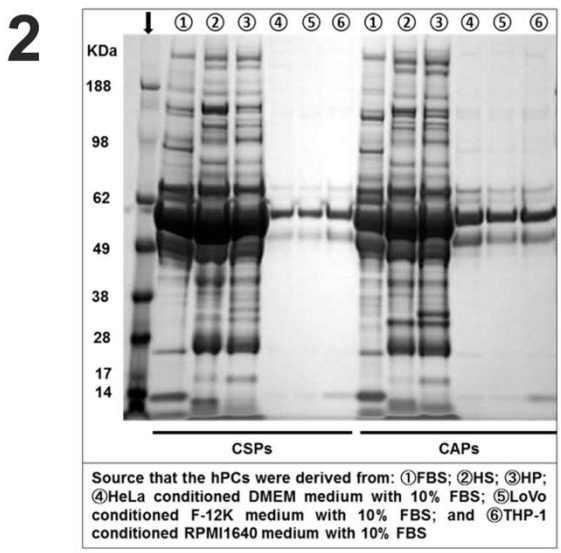

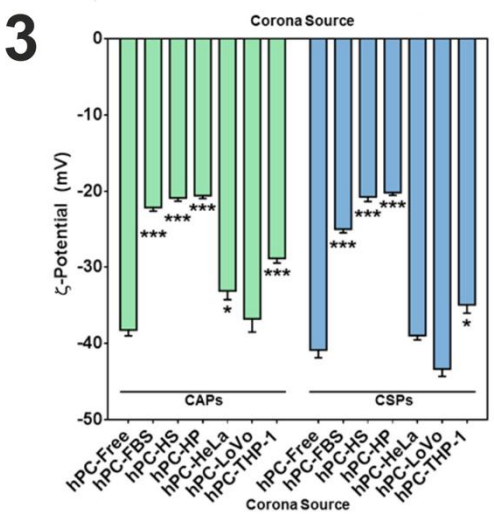

Fig. 3. Versatility of capsule shape and surface charge quenching due to capsule opsonization with components of physiological environment.

Panel 1: Morphology of differently shaped multilayer capsules. (A) structured illumination microscopy, (B) transmission electron microscopy, and (C) atomic force microspy images of polyethylene glycol (PEG) capsules with different shapes: (A1−A3) small spherical; (B1−B3) small rod-like; (C1−C3) large spherical; and (D1−D3) large rod-like. Adapted from Song *et al.*[82].

Panel 2: Sodium dodecyl sulfate-polyacrylamide gel electrophoresis (SDS-PAGE) images of separated corona proteins derived from various environments on core−shell particles (CSPs) and hollow capsules (CAPs). The reference is indicated by the arrow. Adapted from Dai *et al.*[102].

Panel 3: ζ-Potential of poly(methacrylic acid) (PMA) CAPs or CSPs with or without protein coronas derived from various environments. * $p < 0.05$, *** $p < 0.001$ versus the column of "hPC-Free" (one-way ANOVA Dunnett's multiple comparison test). Adapted from Dai *et al.*[102].

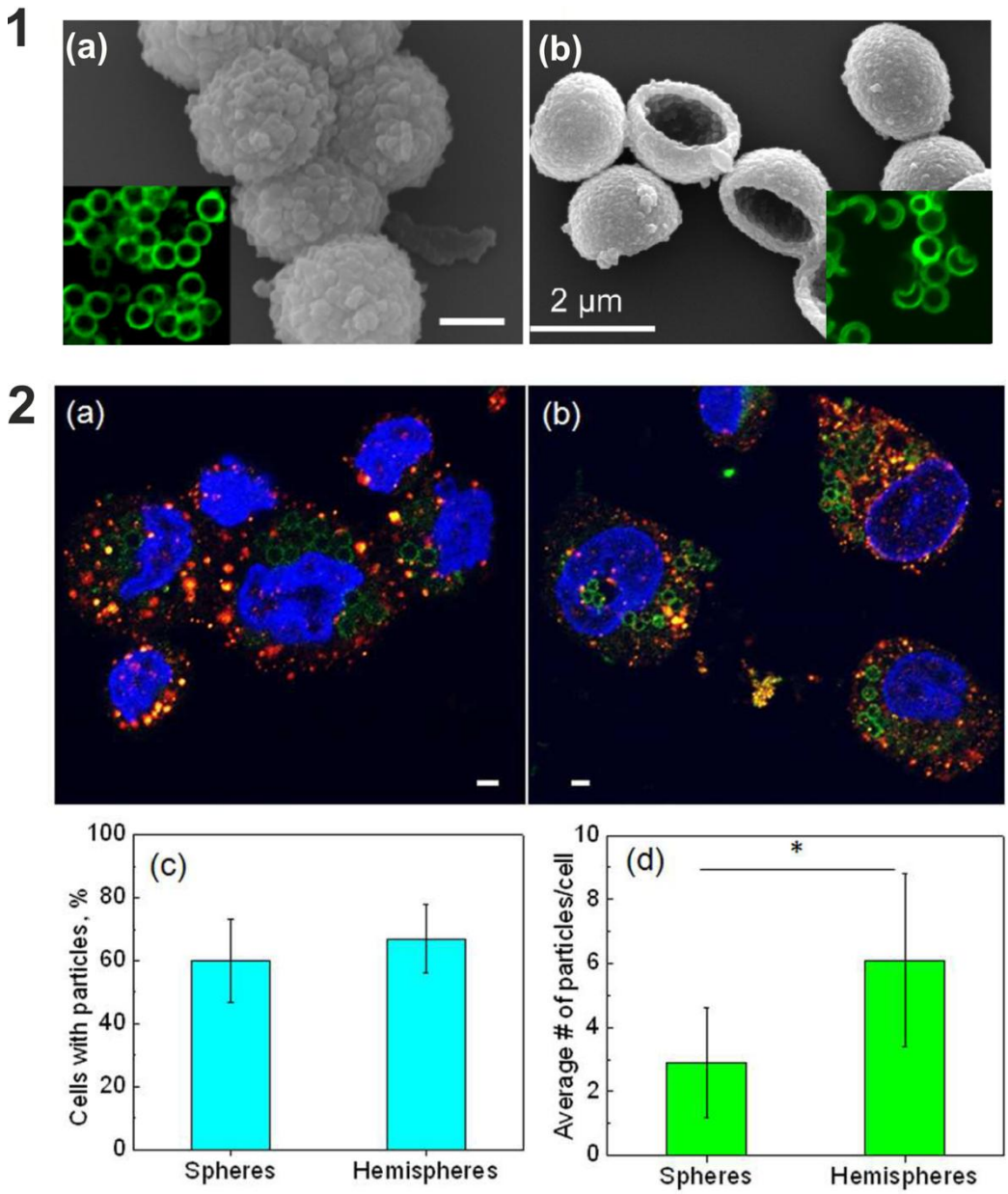

Fig. 4. Shape-dependent capsule uptake.

Panel 1: Scanning electron and confocal microscopy images (represented in insets) of hollow multilayer poly(N-vinylpyrrolidone)/tannic acid $(PVPON/TA)_n$ capsules of (a) spherical (25.5-bilayer shells) and (b) hemispherical shapes. Scale bar is 1 μm in image (a). Adapted from Chen *et al.* [68].

Panel 2: Confocal sections of THP-1 cells with internalized (a) spherical and (b) hemispherical $(PVPON/TA)_{15.5}$ particles. Scale bar is 2 μm. (c) Percentage of cells with internalized $(PVPON/TA)_{15.5}$ particles. (d) Average numbers of the spherical and hemispherical $(PVPON/TA)_{15.5}$ particles internalized per cell (*$p < 0.005$). HeLa cell growth in the presence of (PVPON/TA) capsules at various hollow capsule-to-cell ratios measured by cell counting at 1-, 2-, 3-day intervals. A549 cell growth in the presence of (PVPON/TA) capsules after 3 days of incubation. Adapted from Chen *et al.*[68].

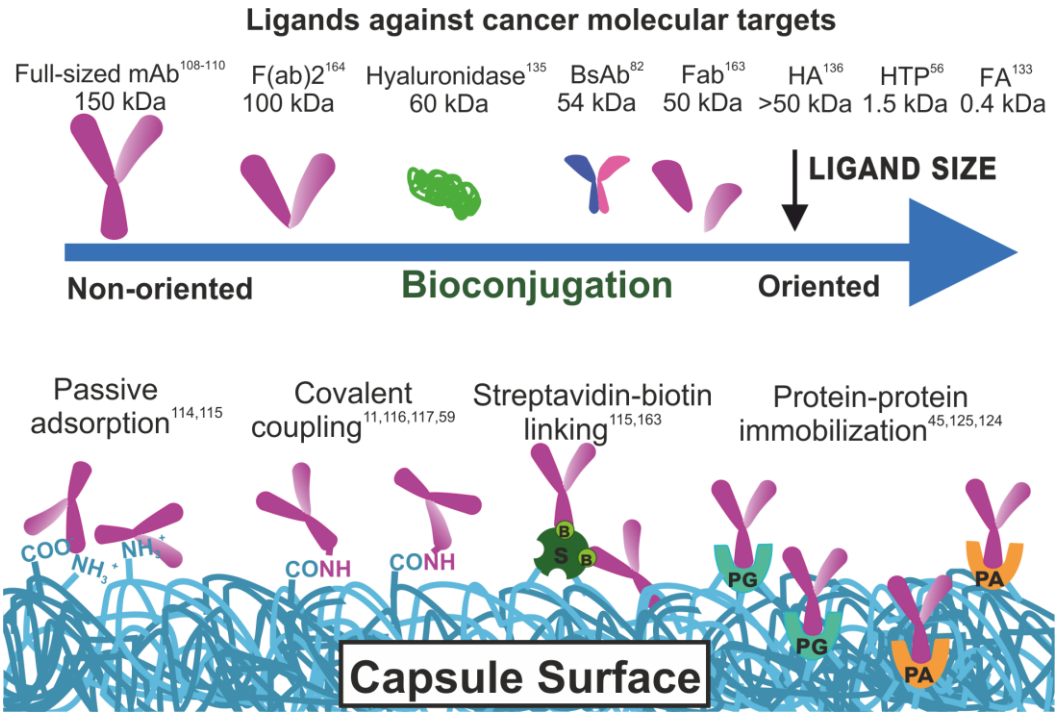

Fig. 5. Biofunctionalization and vectorization of the multilayer capsule surface: a variety of ligand entities and bioconjugation approaches that assume non-oriented and oriented deposition of the vector molecules, e.g., antibodies, that have been successfully used in targeted delivery of the capsules to cancer cells.

Abbreviations: mAb, monoclonal antibody; F(ab)2, F(ab)2 fragments of a monoclonal antibody; BsAb, bispecific antibody; Fab, Fab fragments of a monoclonal antibody; HA, hyaluronic acid; HTP, IPLVVPL hepsin-targeting peptide; FA, folic acid; PA, protein A; PG, protein G; SA, streptavidin; B, biotin.

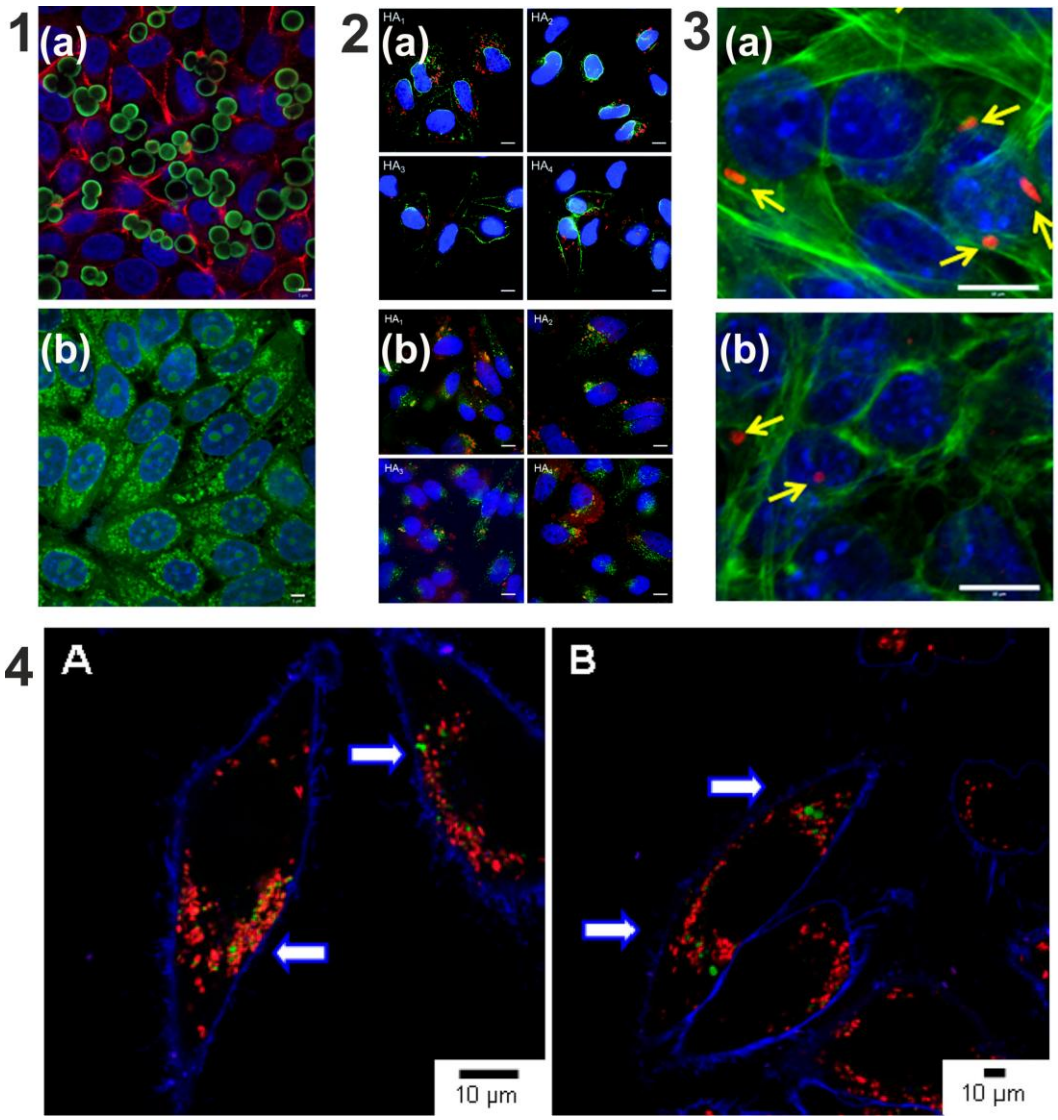

Fig. 6. Capsule uptake and intracellular fate in cancer cells.

Panel 1: (a) Confocal images showing biocompatible poly(sodium 4-styrene sulfonate)/poly(allylamine hydrochloride) PSS/PAH microparticles, with green fluorescent fluorescein isothiocyanate (FITC) in their walls with $(PSS/PAH)_3$ layer sequence, uptake by human cervix adenocarcinoma HeLa cells. Image size 11 µm; nuclei labelled with Hoeschst 33, 352 (blue), the actin of cytoskeleton is labeled in red. (b) Biodegradable chitosan/pectin (CHI/PEC) microparticles uptake by HeLa; nuclei labelled with Hoechst are stained in blue and the diffused green fluorescent shows the polymers degradation. Scale bar 5 µm. The cells were co-incubated with core/shell capsules for 3 h. Adapted from Vergaro *et al.*[85].

Panel 2: (a) Cell internalization of Alexa Fluor F633-labeled hyaluronic acid (HA) capsules with different stiffness in human cervix adenocarcinoma HeLa cells, as determined by deconvolution microscopy. Cells were incubated with capsules (red) at a capsule to cell ratio of 100: 1 for 24 h at 37°C. Cell membranes were stained with Alexa Fluor 488-Wheat Germ Agglutinin (green) and nuclei were counterstained with Hoechst 33342 (blue). Scale bars are 10 mm. Adapted from Sun *et al.*[98]. (b) Intracellular distribution of Alexa Fluor F633-labeled HA capsules with different stiffness in HeLa cells as determined by deconvolution microscopy. Cells were incubated with capsules (red) at a capsule to cell ratio of 100:1 for 24 h at 37 °C. Lysosomes were immunostained with anti-LAMP1 antibody (green), and nuclei were counterstained with Hoechst 33342 (blue). Scale bars are 10 µm. Adapted from Suppl. Materials of Sun *et al.* [98].

Panel 3: Confocal images of 4T1 breast cancer cells after incubation with poly(methacrylic acid)/poly(N-vinylpyrrolidone) $(PMAA\_PVPON)_5$ spherical (a) or discoidal shells (b) for 24 h. Arrows indicate the particles associated with the cells. The capsule shells are labeled red with Alexa Fluor 568. The cell nuclei and cytoskeletons are shown in blue (DAPI) and green (Phalloidin 488), respectively. The scale bar is 10 µm in all images. Adapted from *Kozlovskaya et al.*[89].

Panel 4: Colocalization studies of hydroxy ethyl starch-folic acid fractioned (HES-FA-F) nanocapsules and lysosomes (white arrows) in human cervix adenocarcinoma HeLa cells after 20 h (A) and 40 h (B). The cell membrane is pseudocolored in blue (CellMask Deep Red), HES-FA-F in red, and the lysosomes in green. Adapted from Baier *et al.*[104].

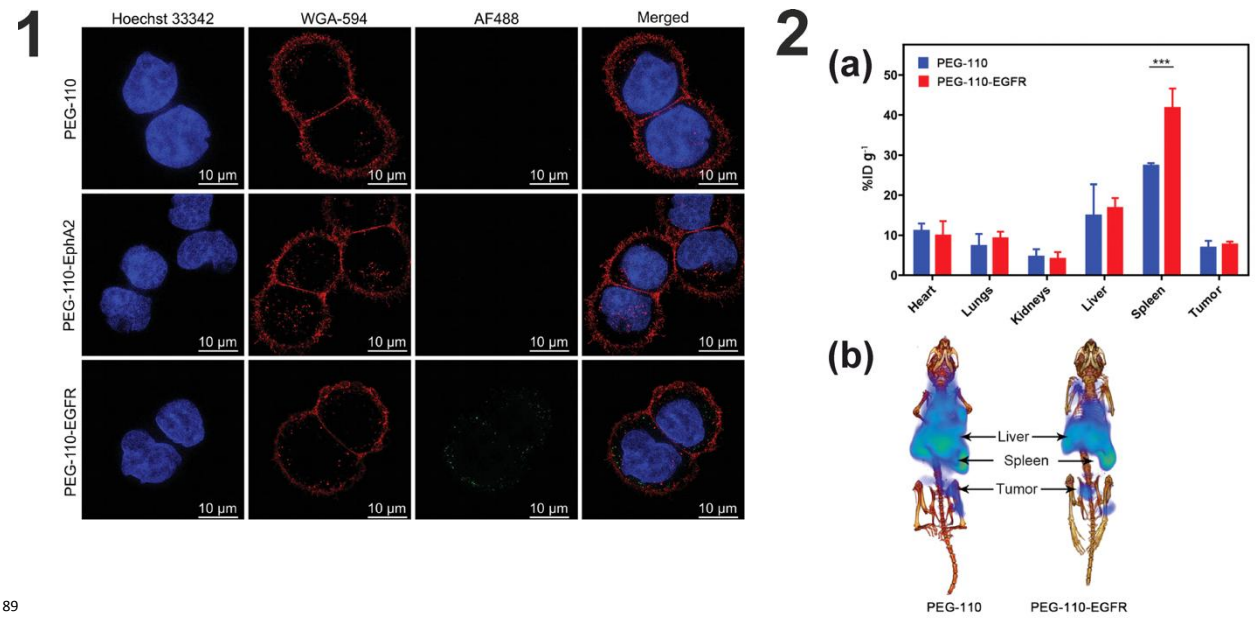

89

Fig. 7. Cell internalization *in vitro*, biodistribution, and tumor accumulation of capsules functionalized with bispecific antibodies (bsAbs) against epidermal growth factor receptor (EGFR).

Panel 1: Super-resolution microscopy images of MDA-MB-468 cells incubated with PEG-110, PEG-110-EphA2, and PEG-110-EGFR particles. BsAbs (40 µg) were incubated with 163 µg PEG-110 particles in 150 µL of Dulbecco phosphate-buffered saline (DPBS) at 4°C for 15 h before incubation with cells. The cell nuclei and membranes were stained with Hoechst 33 342 (blue) and Wheat germ agglutinin Alexa Fluor 488 conjugate (WGA-AF594, red), respectively. The particles were fluorescently labeled with Alexa Fluor 488 (green). The cells were incubated with the particles (8.15 pg of particles per cell) at 37°C for 24 h. Reprinted from Cui *et al.* [126]

Panel 2: (a) *In vivo* biodistribution and tumor accumulation of both PEG-110 and PEG-110-EGFR particles 24 h after injection of ^{64}Cu-labeled PEG-110 and ^{64}Cu-labeled PEG-110-EGFR particles in mice bearing subcutaneous MDA-MB-468 tumors, highlighting increased spleen uptake as a result of the bsAb modification; the data are reported as percentage of injected dose per gram of tissue (%ID g^{-1}). Data represent means ± standard deviations based on triplicate experiments (two-way ANOVA using Tukey's multiple comparisons test, ***$p < 0.001$). (b) Representative positron emission tomography-computed tomography (PET-CT) images 48 h after injection of ^{64}Cu-labeled PEG-110 and ^{64}Cu-labeled PEG-110-EGFR particles with highlights for liver, spleen, and tumor uptake. PEG-110-EGFR particles were obtained by incubating BsAbs (20 µg) with PEG-110 particles (templated from 2 mg of MS-110, 2.6×10^{12} particles). Adapted from Cui *et al.* [126]

Table 1 – Most frequently used model cancer lines and capsule designs in capsule–cell interaction studies

Cell line	Capsule structure	Size, μm	Shape	Rigidity	ζ-potential, mV	Modification	Vectorization	Uptake; intracellular fate	References
Human cervix adenocarcinoma	Shell	~3	Spherical	Soft	~ – 30 - – 36	–	No additional modification surface is formed by HA	Association, internalization, uptake observed; lysosomes	98
HeLa	Shell	~4-9	Spherical	Soft	~ – 30	FITC-BSA encapsulated; FITC-dextran	LMWHA peptide at the surface	Uptake, CD44-receptor-mediated endocytosis; perinuclear region	26
	Shell	~3.5	Spherical	Soft	Positively charged	PEI/siRNA; PEI/DNA polyplexes encapsulated	–	Uptake; lysosomes (nonbiodegradable), cytosol (biodegradable)	23
	Shell	~0.2 – 0.3	Spherical	Soft	~ – 12 - – 27	–	Folic acid at the surface	FRα-mediated uptake	104
	Shell	~1.6	Spherical	Soft	~ – 8 ~ – 18 ~ – 41	Alexa Fluor 488	–	Uptake	148
	Core	2-50	Spherical	Rigid	–	Alexa Fluor 488	Folic acid	Specific particle–cell association	133
	Shell	~4-5	Spherical	Soft	~ + 15 ~ + 25	SNARF-1-dextran encapsulated	–	Uptake observed; lysosomes	77
	Shell	~2.1	Spherical	Soft	~ – 10 - – 38	Alexa Fluor 633	Hyaluronic acid	Negligible association of PEG and PHPMA capsules; low fouling of HA capsules	105
	Shell	~3-4	Spherical	Soft	~ – 13	Cisplatin, PAH-FITC encapsulated	–	Uptake; intracellular compartment	85
	Core-shell			Rigid					
	Core-shell			Rigid					
Human breast adenocarcinoma	Shell	~5.4	Spherical	Soft	~ – 20	BSA, DOX encapsulated	–	Internalization, uptake; cytoplasm and nucleus	38
MCF-7	Shell	~3-4	Spherical	Soft	~ – 13	Cisplatin, PAH-FITC encapsulated	–	Uptake; intracellular compartment.	85
	Core-shell			Rigid					
	Shell	0.7	Cubical	Soft	~ – 17 - – 19	DOX; FITC encapsulated	FITC-labeled IPLVVPL hepsin-	Internalization and uptake *Larger hydrogels were internalized	56

							targeting peptide	more efficiently. The internalization of small-sized hydrogels was cell-specific (internalization efficiency, ~10-70%). The peptide-modified PMAA hydrogels underwent higher uptake.	
		2					No surface modification	Moderate internalization of the capsules of both sizes	
Human breast adenocarcinoma	Shell	~3-4	Spherical	Soft	–	Gold NPs, FITC, TRITC in the shell	–	Lipid-raft-mediated macropinocytosis; heterophagolysosomes	149
MDA-MB-231	Shell	~2.1	Spherical	Soft	~ – 10 - – 38	Alexa Fluor 633	Hyaluronic acid	High targeting specificity of HA capsules	105
Human breast adenocarcinoma MDA-MB-468	Shell	0.11	Spherical	Rigid	~ – 10 - 0	Alexa Fluor 488; Alexa Fluor 633	Anti-PEG/anti-EGFR bispecific Abs at the surface; PEG chains of various lengths at the surface	Specific particle–cell association, internalization; inside cell membrane	126
	Shell	~0.5 ~1.1 ~1.3*0.2 ~4.2*0.2	Small spherical Large spherical Small rod Large rod	Soft	– 13	Alexa Fluor 488; Alexa Fluor 647	anti-PEG/anti-EGFR bispecific Abs at the surface; PEG chains of various lengths at the surface	Association, specific cellular association; internalization; uptake	82
Human ductal carcinoma BT474	Shell	~2.1	Spherical	Soft	~ – 10 - – 38	Alexa Fluor 633	Hyaluronic acid	Low fouling of HA capsules.	105
Human breast adenocarcinoma	Core-shell	~3	Spherical	Rigid	~ – 10	–	Alexa488-IgG at the surface	Macropinocytosis for all capsule types	114

SKBR-3					~ + 5 - + 15		Alexa488-IgG and PEI 25 kDa or 750 kDa at the surface	Effectiveness of internalization was higher	
Human lung carcinoma	Shell	~3-4	Spherical	Soft	–	Gold NPs, FITC, TRITC in the shell	–	Phagocytosis; heterophagolysosomes	[149]
A549	Shell	~4-5	Spherical	Soft	~ + 15 ~ + 25	SNARF-1-dextran encapsulated	–	Uptake observed; lysosomes	[77]
Human bone marrow neuroblastoma	Shell	~4-5	Spherical	Soft	~ + 15	SNARF-1-dextran encapsulated	–	Low uptake	[77]
SH-SY5Y					~ + 25				
Human ovarian adenocarcinoma	Shell	0.7	Cubical	Soft	~ – 17 - – 19	DOX; FITC encapsulated	FITC-labeled IPLVVPL hepsin-targeting peptide	Internalization; uptake. Peptide-modified PMAA hydrogels underwent higher uptake (internalization efficiency, ~30–75%).	[56]
SK-OV-3									
Human prostatic adenocarcinoma	Shell	0.7	Cubical	Soft	~ – 17 - – 19	DOX; FITC encapsulated	FITC-labeled IPLVVPL hepsin-targeting peptide	Low internalization (internalization efficiency <20%)	[56]
PC-3									
Human hepatocellular carcinoma	Shell	~3.5	Spherical	Soft	–	RBITC	–	Internalization, uptake. Faster uptake of discoidal capsules. Capsule shape does not significantly affect internalization	[94]
HepG2		~3.3*1.3	Discoidal						
		~4.5-5	Spherical	Soft	~ – 20 - – 25	FITC	–	Microcapsules with large number of layers does affects cytoskeleton structure	[165]

Human colon adenocarcinoma LIM1899	Shell	0.6 (pH 4) - 0.85 (pH 8)	Spherical	Soft	– 58	DOX encapsulated; Alexa Fluor 633	–	Internalization, uptake; membrane-enclosed compartments and late endosomes or lysosomes. DOX accumulates in the nucleus after capsules are internalized	88,150
	Shell	~2	Spherical	Soft	– 34	Alexa Fluor 488; Alexa Fluor 633	Humanized A33 monoclonal antibody	Cell-specific interaction in the case of Ab-fucntionalized capsules with and without the protein corona	59
					– 29 ± 1 (10% serum) – 25 ± 4(50% serum), – 24 ± 2 (100% serum)		Humanized A33 monoclonal antibody + protein corona		
Human promyeloblast leukemia HL-60	Shell	~5	Spherical	Soft	Negatively charged	RITC-PAH	–	Association with negatively charged capsules is 54.03%±9.22% at the exposure dose of 10 capsules per cell	96
	Core-shell			Rigid	Positively charged			Positively charged capsules were observed to be less interactive	
Mouse colon carcinoma CT-26	Shell	~0.5	Spherical	Soft	–	Pt(IV); PLL-RhB and PLL-FITC	–	Internalization, uptake; lysosomal compartments.	29
Mouse lymphoma RMA	Shell	3.0	Spherical	Soft	– 30	Alexa Fluor 488 or Alexa Fluor 647 labeled BSA	Y3 and 5D3 antibody (oriented coupling)	Cell-specific interaction, internalization in the case of capsules functionalized with Y3; 5D3-modified capsules exhibited no binding	45

Abbreviations: HA, hyaluronic acid; FRα, folate receptor; LMWHA , low-molecular-weight hyaluronic acid ; DNA, deoxyribonucleic acid; PEG, poly(ethylene glycol); EGFR, epidermal growth factor receptor; PHPMA, poly(N-(2-hydroxypropyl)-methacrylamide); PMAA, poly(methacrylic acid); Ab, antibody; FITC, fluorescein isothiocyanate; BSA, bovine serum albumin; PEI, polyethyleneimine; siRNA, small interfering ribonucleic acid; SNARF-1, pH-sensitive fluorescent dye; PAH, polyallyamine hydrochloride ; DOX, doxorubicin; NPs, nanoparticles; TRITC, tetramethylrhodamine; RBITC, rhodamine B isothiocyanate; RhB, rhodamine B ; PLL, poly-L-lysine.